previously (29). In brief, total RNA was prepared using TRIzol Reagent (Invitrogen). Twenty micrograms of total RNA was fractionated by electrophoresis in a 0.8% agarose gel containing formaldehyde. The separated RNAs were then transferred onto Hybond-N$^+$ membranes (Amersham Biosciences) in 10 x SSC. After UV-cross-linking, the membranes were subjected to prehybridization and hybridization in a solution containing 0.5 M sodium phosphate (pH 7.2), 1 mM EDTA, and 7% SDS at 65 °C. A probe prepared by radiolabeling with [α-^{32}P]dCTP using a Random Prime-DNA labeling kit (Takara Shuzo Co.) was added, and hybridization was carried out overnight. Membranes were then extensively washed with a washing buffer (2× SSC (1× SSC = 0.15 M NaCl and 0.015 M sodium citrate), 0.1% SDS) at 65 °C, and the signals were visualized with a Bio-Image Analyzer, FLA-2000 (Fuji Film). The probes used to detect murine *stam1*, *stam2*, and glyceraldehyde-3-phosphate dehydrogenase (*gapdh*) mRNAs were described elsewhere (29, 30).

Immunofluorescence Microscopy and Immunostaining—Cells were seeded into 35-mm glass-bottomed dishes (MatTek Co.) at a density of 1×10^5 cells/dish 1 day before the transfection. DsRed1-Eps15 was then introduced as described above. After 48 h, the cells were washed twice with phosphate-buffered saline, fixed with 4% paraformaldehyde for 15 min, permeabilized for 10 min with phosphate-buffered saline containing 0.1% Triton X-100, and then blocked for 30 min with phosphate-buffered saline containing 10% fetal calf serum and 0.1% Triton X-100. For immunostaining, the fixed samples were incubated with the indicated primary antibodies, washed 3 times, and further probed with the secondary antibodies (anti-rabbit, -mouse, and -goat IgG antibodies conjugated with Alexa 488, Alexa 594, and Alexa 350, respectively (Molecular Probes)). The microscopic images were examined using the Leica DMIRBE microscope system with a PL FLUOTAR 100×/1.30–0.60 oil immersion objective.

Metabolic Labeling of Cellular Proteins—For pulse-chase experiments, HRSd and 293T cells that had been transiently transfected with the indicated plasmids using FuGENE™ 6 were radiolabeled with the Pro-mix $_L$-[^{35}S] in Vitro Cell Labeling Mix at a concentration of 100 μCi/ml (Amersham Biosciences) in Met/Cys-free Dulbecco's modified Eagle's medium (Invitrogen) supplemented with 10% fetal calf serum that had been predialyzed against phosphate-buffered saline for 30 min. At the end of the pulse-labeling period, the cells were washed and chased for the indicated times in complete Dulbecco's modified Eagle's medium supplemented with methionine and cysteine. Cells were collected by centrifugation, and the lysates made from them were subjected to further immunoprecipitation assays. Radioactivity was visualized and analyzed using Science Lab 2001 Image Gauge Version 4.0 software (Fuji Film).

RESULTS

Establishment of hrs-deficient Cell Lines by Gene Targeting—The *hrs* knock-out mice have an embryonic lethal phenotype, as described previously (26, 31). To analyze the biological significance of Hrs *in vivo*, we sought to generate conditional *hrs* gene-targeted mice. The targeting construct was designed to delete exon 6 of the *hrs* genomic sequence (Fig. 1*A*). Exon 6 (*E6*) codes for amino acids 139–156, and therefore, the resultant *hrs* gene-targeted allele was expected to code for an Hrs protein with a minimal N-terminal portion that lacked part of the VHS domain (amino acids 1–138). After a positive-negative selection screen, several recombinant ES clones were selected and injected into blastocysts. The chimeric mice obtained were crossed with each other to obtain heterozygous mice ($hrs^{+/floxP}$). The genotype was confirmed both by Southern blot and genomic PCR analyses (Fig. 1, *B* and *C*). Although the heterozygous mice were viable and fertile, when they were intercrossed we did not obtain viable $hrs^{floxP/floxP}$ offspring. Indeed, our timed breeding experiments revealed that the $hrs^{floxP/floxP}$ embryos were not viable after E10.5 (data not shown). We concluded that the conditional hrs^{floxP} allele was nonfunctional. Although we were unable to establish cell lines from our original *hrs* gene knock-out mice (26) because the allele still produced a C-terminal-truncated Hrs (amino acids 1–454), these new mutant $hrs^{floxP/floxP}$ embryos were ideal for preparing mouse embryonic fibroblastoid cells (MEFs). We successfully prepared MEFs from E9.5 embryos, and among randomly prepared MEF cells only the $hrs^{floxP/floxP}$ MEFs failed to survive after a few passages; in comparison, wild-type MEFs survived for many passages. We immortalized the $hrs^{+/+}$ and $hrs^{floxP/floxP}$ MEFs using the SV40 large T antigen. We obtained an immortalized cell line carrying the $hrs^{floxP/floxP}$ genotype and a control $hrs^{+/+}$ cell line, MEFw. Next, the *hrs* gene and the neomycin resistance gene (*neo*^{r}) were fully inactivated by deleting the gene segment encoding exon 6. By introducing the transient expression of Cre recombinase into the cells carrying the $hrs^{floxP/floxP}$ genotype, we obtained a cell line, HRSd, with the $hrs^{\delta/\delta}$ genotype. Deletion of the region flanked by the two loxP sequences was confirmed by genomic PCR (Fig. 1*D*). Although the δ allele could potentially have produced an N-terminal 138-amino acid fragment, the defective expression of

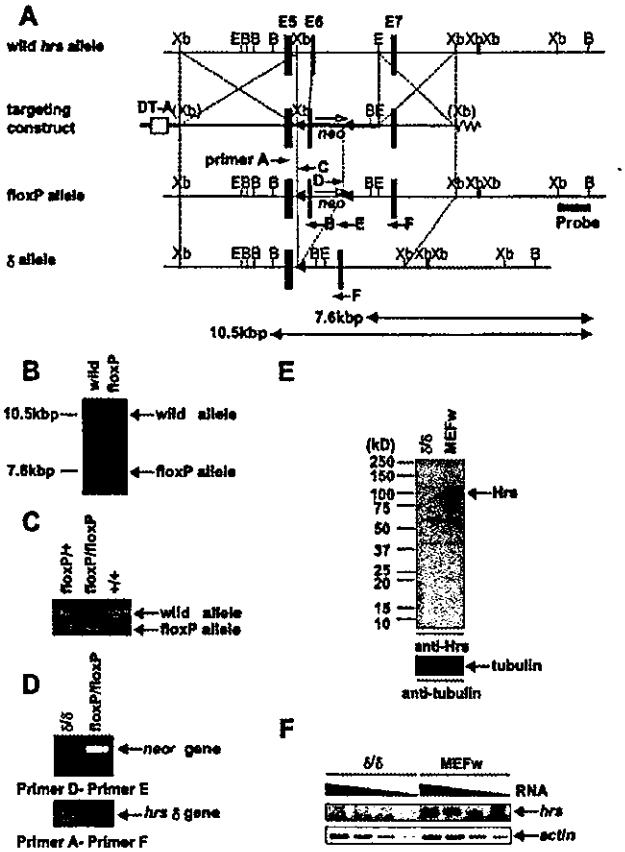

FIG. 1. **Targeted disruption of the *hrs* gene.** *A*, schematic restriction maps of the wild-type, targeting construct, and mutant alleles. The mutated allele is shown in its floxP and δ forms. *E5*, *E6*, and *E7* stand for exons 5, 6, and 7 of the *hrs* genome. *B*, *Xb*, and *E* stand for the restriction sites for BamHI, XbaI, and EcoRI, respectively. The 3′ probe used for the analytical Southern blot is shown. Primer pairs used to detect the targeted allele are shown; primers A and C for the first loxP-containing joint region and primers D and E for the neomycin-resistance gene (*neo*^{r}). *B*, a representative genomic Southern blot analysis for the wild-type (*wild*) and recombinant (*floxP*) alleles from ES cells. Genomic DNAs extracted from ES cell clones were digested with BamHI. After gel separation and blotting, the filter was hybridized with the 3′ probe. The 10.5- and 7.6-kilobase pair (*kbp*) fragments indicate wild-type and recombinant alleles, respectively. *C*, PCR-genotyping analysis of *hrs* in embryonic cell lines derived from wild-type (+/+), heterozygous (floxP/+), and homozygous (floxP/floxP) embryos. The lengths of the PCR fragments are 330 and 160 bp for the wild-type and mutant alleles, respectively. *D*, Cre-mediated deletion of *neo*^{r}. An immortalized fibroblastoid cell line with the floxP/floxP genotype was treated with Cre, and PCR analyses of the *neo*^{r} and *hrs* δ gene were performed. *E*, immunoblot analyses of the Hrs protein in an immortalized knock-out (δ/δ) and a control cell line (MEFw). *F*, semiquantitative RT-PCR analyses of the *hrs* and *β-actin* expression in HRSd and MEFw cells. Templates were prepared to make a series of 3-fold dilutions.

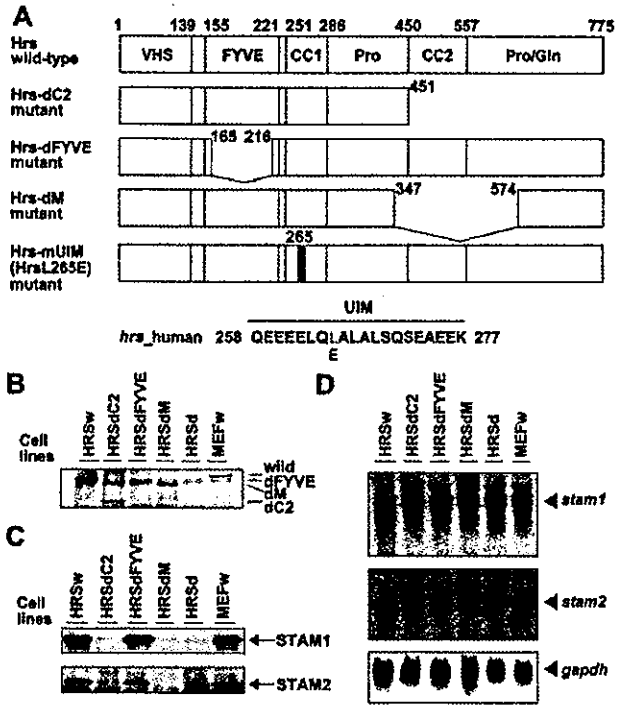

FIG. 2. **Decreased STAM1 and STAM2 in HRSd and in the presence of Hrs mutants lacking the ability to associate with the STAMs.** *A*, structures of wild-type Hrs and four mutants: *VHS*, *FYVE*, coiled-coil (*CC1* and *CC2*), proline-rich (*Pro*), and proline/glutamine-rich (*Pro/Gln*) domains. Hrs-dC2 lacks the C-terminal 326 amino acid residues, Hrs-dFYVE lacks the FYVE domain, and Hrs-dM lacks the region spanning $Pro^{348}$and Met^{573}. Hrs-mUIM (HrsL265E) carries a leucine (*L* in *red*) to glutamic acid (*E* in *blue*) point mutation at amino acid 265. *B*, the Hrs-deficient cell line (HRSd) and its sublines stably expressing wild-type Hrs, Hrs-dC2, Hrs-dFYVE, and Hrs-dM, respectively, were examined for the expression of Hrs proteins. The MEFw cell line was the control. Rabbit anti-Hrs antibody was used to detect the Hrs proteins. *C*, protein levels of STAM1 (*upper panel*) and STAM2 (*lower panel*). Lysates from the Hrs-deficient cell line (HRSd) and its sublines were used for immunoprecipitation and immunoblotting with an anti-STAM1 monoclonal antibody (TUS-1) and an anti-STAM2 monoclonal antibody (ST2–2), respectively. *D*, mRNA expression of STAM1 and STAM2 in HRSd and its sublines. Total RNAs were used for the detection of STAM1 (*stam1*) and STAM2 (*stam2*) mRNA. mRNA levels of the glyceraldehyde-3-phosphate dehydrogenase gene (*gapdh*) were monitored as the control.

both Hrs and the smaller protein in HRSd cells was confirmed with anti-Hrs antisera (Fig. 1*E*). We then performed RT-PCR experiments to determine if any mRNA containing the intact coding region within *hrs* could be detected. However, we could not detect any mRNA for *hrs* in HRSd cells (Fig. 1*F*). We, therefore, concluded that HRSd cells display a null phenotype. A gross microscopic analysis showed both the HRSd and MEFw cell lines displayed a similar flat cell shape (data not shown).

Stability of STAM1 and STAM2 Is Dependent on Hrs—Our previous experiments indicated that STAM1 and STAM2 bind directly to Hrs and are involved in the vacuolar membrane transport machinery (4, 32). To analyze the function of Hrs and its subdomains, we established HRSd sublines stably expressing wild-type (HRSw) or the dC2 (HRSdC2), dFYVE (HRSdFYVE), or dM (HRSdM) mutants of Hrs (Fig. 2, *A* and *B*). We first examined the level of the Hrs-associated proteins STAM1 and STAM2 in the mutant and MEFw lines. Although significant STAM1 protein was detected in the HRSw and MEFw cells, only minimal STAM1 was detected in HRSd cells (Fig. 2*C*). Interestingly, HRSdFYVE cells displayed a level of STAM1 similar to the level expressed by HRSw and MEFw cells, whereas the dC2 and dM mutants exhibited severely reduced levels of STAM1 (Fig. 2*C*). A similarly defective level of STAM2 was observed in HRSd, HRSdC2, and HRSdM cells (Fig. 2*C*). These results suggest that Hrs contributes to the levels of both STAM1 and STAM2 and that the Hrs region responsible for this contribution lies within amino acids 451–574, which includes the CC2 domain.

We next investigated the mechanism underlying the severely decreased levels of STAM1 and STAM2 in HRSd, HRSdC2, and HRSdM. To determine whether the suppression of STAM1/STAM2 was controlled at the transcriptional or post-transcriptional level, mRNAs prepared from HRSd and its sublines were subjected to Northern blotting. The results clearly indicated that there was little if any difference in the mRNA expression of STAM1 or STAM2 among these cell lines (Fig. 2*D*). Taken together, these results indicate that the decrease in STAM levels in the dC2 and dM Hrs mutants was post-transcriptional and was due to protein instability.

Degradation of STAM1 Is Regulated by the STAM Interaction Domain of Hrs—Since Hrs is involved in the vacuolar membrane transport machinery, we speculated that Hrs might contribute to the stability of the STAM1 protein. Therefore, we tested the possibility that Hrs is critical in regulating STAM1 degradation. To examine this possibility, HRSd cells were transiently transfected with expression vectors encoding epitope-tagged STAM1 (STAM1-V5) and Hrs. We monitored STAM1 degradation in the presence of cycloheximide (to stop *de novo* protein synthesis) by Western blotting. Although the initial level of STAM1 decreased significantly in the presence of Hrs, the degradation rate accelerated significantly in its absence (Fig. 3*A*). A similar accelerated degradation in the absence of Hrs was detected when STAM2 was tested (data not shown).

To further clarify the rate of STAM1 degradation, we performed a pulse-chase analysis of STAM1 protein expression in the presence or absence of Hrs. Hrs-deficient HRSd cells were co-transfected with a STAM1 expression plasmid along with wild-type Hrs or control vectors, and the cells were then metabolically radiolabeled. A similar level of radiolabeled STAM1 protein was detected in the presence or absence of Hrs just after the labeling period (time 0), suggesting comparable protein synthesis for STAM1 irrespective of Hrs (Fig. 3*B*). In the presence of Hrs, the radiolabeled STAM1 was slightly increased at the initial 2-h time point after the chase, probably reflecting the ongoing *de novo* protein synthesis from the incorporated amino acid pool, as previously reported (33, 34). At 8 h after the chase, STAM1 protein decreased to 30% of the initial level; in contrast, in the presence of Hrs, 80% of the initial amount of STAM1 was observed. We also investigated the effect of various Hrs subdomains on the stability of STAM1. After transient transfection with the STAM1 and Hrs expression constructs, irrespective of whether wild-type or mutant Hrs was used, ~50% of the cells co-expressed STAM1 and Hrs, with a negligible portion expressing only STAM1 (data not shown). Based on this observation, we concluded that this assay was useful for monitoring the effect of Hrs on STAM1 instability. In the absence of Hrs, a relatively fast decrease of STAM1 to 40% of its initial level was observed 6 h after the chase, which was similar to its rate of decrease in the presence of the Hrs-dM mutant (Fig. 3*C*). Consistent with our previous experiment, wild-type Hrs resulted in 80% of the radiolabeled STAM1 remaining after the chase. To determine if the UIM domain of Hrs was involved in the degradation of STAM1, we introduced a point mutation into Hrs, in which the leucine residue at amino acid position 265 was replaced by glutamic acid, resulting in this failure of the construct to bind ubiquitin (*Hrs-mUIM*, Fig. 2*A*). However, the degradation rate in the

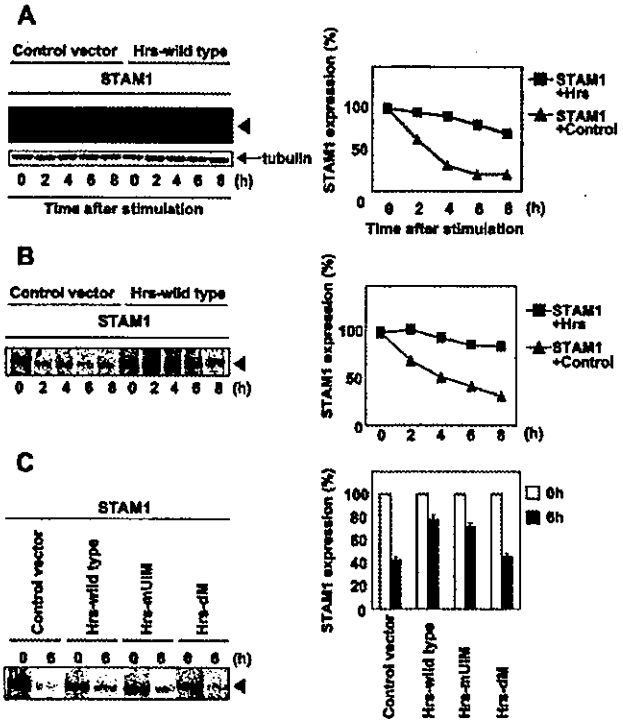

FIG. 3. **Degradation of STAM1 is controlled by Hrs.** *A*, HRSd cells were transfected with the V5-tagged STAM1 expression vector together with Hrs or a control vector. After 48 h in culture, the cells were serum-starved for 1 h and then incubated with 25 μg/ml cycloheximide. The cell lysates were immunoblotted. STAM1-V5 (*arrowhead*) and α-tubulin (tubulin) are indicated. The signal density was analyzed with a FluoroImager, and the relative densities to the initial STAM1 expression level were determined. *B*, HRSd cells were transfected with a V5-tagged STAM1-expression vector and the Hrs or control vectors. After 48 h in culture, the cells were radiolabeled with 100 μCi/ml [^{35}S]methionine/cysteine for 30 min at 37 °C and further cultured for the indicated times. After extensive washes, the STAM1 protein was recovered by immunoprecipitation with the anti-V5 antibody and monitored for radioactivity. Signals from the V5-tagged STAM1 are indicated by *arrowheads*. The amounts of radioactivity were determined. *C*, effect of wild-type Hrs and Hrs mutants on the degradation of STAM1 in HRSd cells. HRSd cells were transfected with STAM1-V5 or the control vector and radiolabeled as described in *B*. Signals from V5-tagged STAM1 are indicated by *arrowheads*. Radioactivity from STAM1 at the 0- and 6-h time points was measured, and the relative protein amount detected by the Imager is shown.

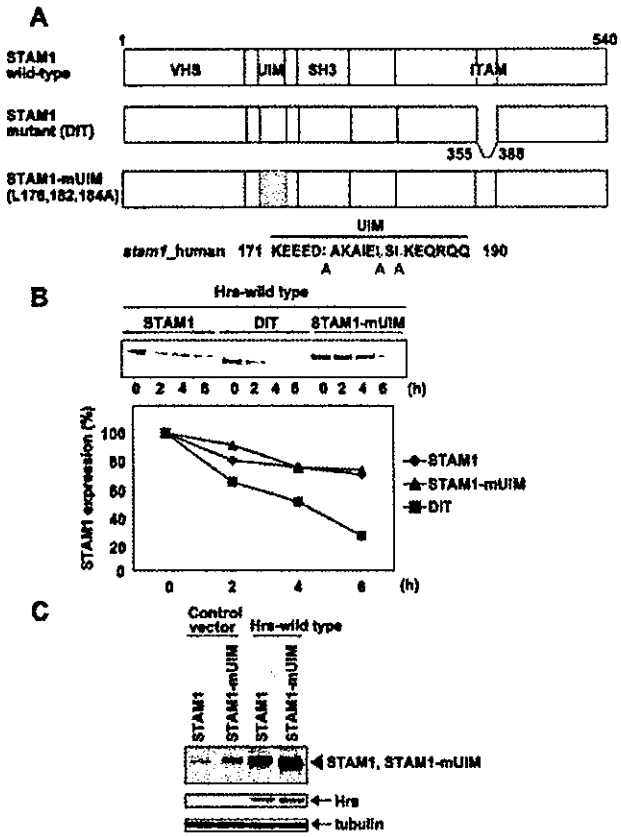

FIG. 4. **Effect of Hrs on the degradation of STAM1 and its mutants in 293T cells.** *A*, schematic structures of wild-type STAM1 and its mutants, DIT, and STAM1-mUIM. *SH3*, Src homology domain. The DIT mutant lacks the ITAM. STAM1-mUIM carries three point mutations in leucines at positions 176, 182, 184, which are replaced by alanines (leucines, *L* in *red*, replaced by alanines, *A* in *blue*). *B*, 293T cells were transfected with Hrs and STAM1-V5, DIT-V5, or STAM1-mUIM-V5. After 48 h in culture, the cells were labeled with 100 μCi/ml [^{35}S]methionine/cysteine for 30 min at 37 °C and chased for the indicated times. The STAM1-V5, DIT-V5, or STAM1-mUIM-V5 was immunoprecipitated with the anti-V5 antibody. The total amount of radioactivity in each lane was determined. *C*, Hrs-deficient cells (HRSd) were transfected with STAM1-V5 or STAM1-mUIM-V5 in combination with control or wild-type Hrs vectors. Lysates were subjected to immunoblotting with anti-V5, anti-Hrs, and anti-tubulin antibodies.

presence of Hrs-mUIM was similar to the result with wild-type Hrs (Fig. 3*C*). These results indicate that Hrs contributes to the protein stability of STAM1, for which the STAM1-association domain of Hrs is required, but the UIM domain of Hrs is not.

STAM1 Stability Is Mediated via Hrs Binding, and the UIM Domain of STAM1 Is Required for Its Stabilization—We next examined which STAM1 subdomains were responsible for the Hrs-mediated stabilization of STAM1. For this study, we used two V5-tagged STAM1 mutants, STAM1-DIT and STAM1-mUIM. STAM1-DIT lacked ITAM, an Hrs binding domain (16), and STAM1-mUIM carried three amino acid substitutions from Leu to Ala at amino acids 176, 182, and 184 in the UIM domain; these substitutions abrogated its ubiquitin binding ability (Fig. 4*A*). 293T cells were transiently co-transfected with wild-type Hrs along with wild-type STAM1 or its mutants. Whereas the level of metabolically radio-labeled STAM1-DIT gradually decreased to about 25% of its initial level during a 6-h chase, wild-type STAM1 and STAM1-mUIM showed less degradation, decreasing only to 80% by 4 h after the chase and then gradually to 70% by 6 h (Fig. 4*B*). Since the DIT mutant could not bind wild-type Hrs, these results suggest that a direct interaction between Hrs and STAM1 is required for the stability of STAM1.

To further examine the effect of Hrs on the degradation/stability of STAM1, we used the HRSd cells. Compared with wild-type STAM1, the amount of STAM1-mUIM was significantly greater, even in the absence of Hrs (Fig. 4*C*). In addition, the expression levels of both STAM1 and STAM1-mUIM were much higher in the presence of Hrs than in its absence (Fig. 4*C*). These results suggest that the UIM domain of STAM1 is essential for the stability of STAM1, and the co-expression of Hrs significantly augments the STAM1 protein stability.

STAM1 Is a Polyubiquitinated Protein and Is Degraded in a UIM-dependent Manner by Proteasomes—Our results to this point indicated that STAM1 could be degraded by either of the two main protein degradation pathways, *i.e.* the lysosomal or ubiquitin-proteasomal pathways (35). To define the degradation pathway of STAM1, we first examined the effects of lactacystin, a potent and selective proteasome inhibitor, and of a lysosome inhibitor, E-64-d, on the stability of STAM1 in the absence of Hrs. HRSd cells were transiently co-transfected with wild-type STAM1 and HA-tagged ubiquitin in the presence or absence of lactacystin. Incubation with lactacystin in-

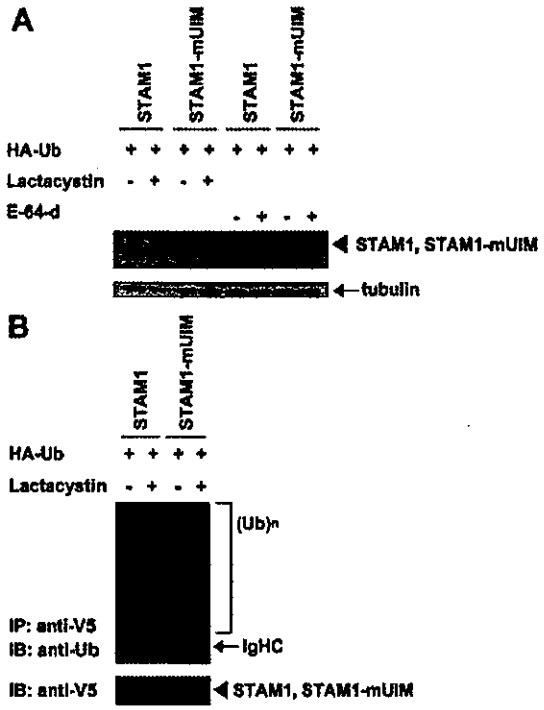

FIG. 5. **STAM1 was degraded by the ubiquitin-proteasome pathway via its UIM.** *A*, HRSd cells were transfected with STAM1-V5 or STAM1-mUIM-V5 in combination with HA-tagged ubiquitin and then cultured with H_2O, 10 μM lactacystin, or 100 μM E-64-d for 10 h. Cells were lysed in 1% Nonidet P-40 cell lysis buffer, and the lysates were used for immunoprecipitation and immunoblotting with the anti-V5 antibody. *B*, immunoprecipitation (*IP*) analysis of STAM1 proteins from 293T cells. 293T cells were transfected with STAM1-V5 or STAM1-mUIM-V5 in combination with HA-tagged ubiquitin and then cultured with H_2O or 10 μM lactacystin for 10 h. Cell lysates were used for immunoprecipitation with the anti-V5 antibody and immunoblotted (*IB*) with the anti-ubiquitin or anti-V5 antibody.

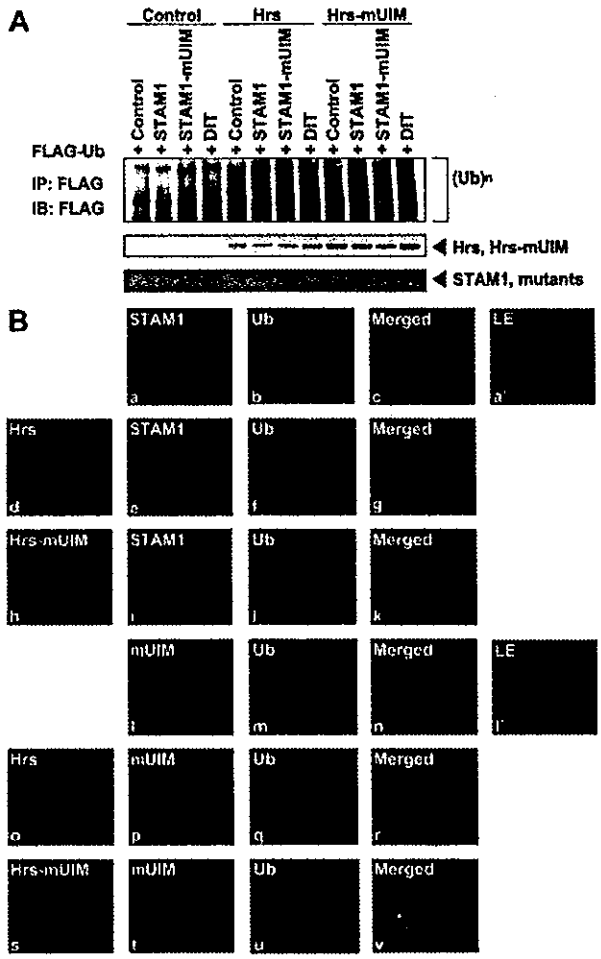

FIG. 6. **Overexpressed Hrs accumulated as a ubiquitinated protein.** *A*, HRSd cells were transfected with the control vector, STAM1-V5, or its mutants in the presence or absence of wild-type Hrs or Hrs-mUIM in combination with FLAG-tagged ubiquitin. Lysates of these cells were used for immunoprecipitation (*IP*) and immunoblotting (*IB*) with the anti-FLAG antibody. Cell lysates were immunoblotted with rabbit anti-Hrs and anti-V5 antibodies. *B*, wild-type Hrs, Hrs-mUIM, STAM1-V5, STAM1-mUIM-V5, and ubiquitin in the early endosome. HRSd cells were transiently transfected with the indicated plasmids. The cells were double- or triple-labeled with the indicated antibodies and fluorescence-conjugated secondary antibodies: Hrs (Alexa 488 (*green*)), STAM1 (Alexa 594 (*red*)), and ubiquitin (Alexa 350 (*blue*)) are shown. Images taken with a longer exposure (*LE*) for *a* and *l* are shown in *a'* and *l'*. *Bars* indicate 20 μm.

creased the amount of wild-type STAM1 protein (Fig. 5*A*). Interestingly, STAM1-mUIM was significantly more stable than wild-type STAM1 even in the absence of lactacystin, and its stability increased profoundly in the presence of lactacystin. On the other hand, E-64-d showed little if any effect on STAM1 stability.

Since protein degradation by proteasomes is regulated by protein ubiquitination, we asked whether STAM1 was ubiquitinated. 293T cells were transiently co-transfected with wild-type STAM1 and HA-tagged ubiquitin. The co-transfected cells were subjected to immunoprecipitation with the anti-V5 antibody, and the ubiquitins in the precipitates were analyzed (Fig. 5*B*). Although the V5 tag contains one lysine residue, our preliminary experiments suggested that this lysine receives little if any modification by ubiquitin (data not shown). As expected, ubiquitin clearly co-precipitated with STAM1. Furthermore, the prior treatment of cells with lactacystin significantly increased the degree of ubiquitination. The protein expression levels of wild-type STAM1 and STAM1-mUIM did not differ significantly in our hands, probably because of the expression of endogenous Hrs in the 293T cells. Collectively, these results suggest that STAM1 is a polyubiquitinated protein, and mutations of its UIM domain severely abolish the ubiquitination.

STAM1·Hrs Complex Is Responsible for Ubiquitin Accumulation on/within the Endosomes—To clarify whether the STAMs and Hrs contribute to the accumulation of cellular ubiquitinated proteins, we co-transfected HRSd cells with the STAM1 and Hrs expression vectors and FLAG-tagged ubiquitin. Whole-cell lysates were then tested for the intracellular accumulation of ubiquitinated proteins. In the absence of Hrs, the introduction of wild-type STAM1 and DIT resulted in little if any increase in the amount of ubiquitin accumulation (Fig. 6*A*). Transfection of STAM1-mUIM slightly increased the ubiquitination. However, the introduction of Hrs caused a marked accumulation of ubiquitinated proteins irrespective of the presence of STAM1. Unexpectedly, a slightly smaller amount of ubiquitins accumulated in the presence of Hrs-mUIM than in the presence of wild-type Hrs even though Hrs-mUIM seemed more stable than wild-type Hrs (Fig. 6*A*, *middle panel*). These results indicate that Hrs is responsible for the intracellular accumulation of ubiquitinated proteins, independent of STAM1.

We next asked whether the presence of STAM1 and Hrs could affect the endosomal localization and accumulation of ubiquitinated proteins. Consistent with our earlier results,

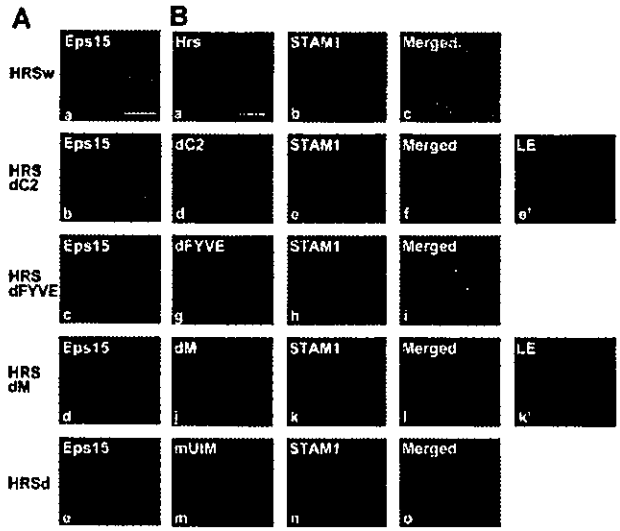

FIG. 7. **UIM mutant of Hrs confers endosome enlargement phenotype.** *A*, early endosome phenotypes detected by Eps15 expression. HRSd and its sublines were transiently transfected with the Eps15 expression vector. Eps15 is shown in *red*. *Bars* indicate 20 μm. *B*, localization of wild-type Hrs, its mutants, and STAM1. HRSd cells were transiently transfected with various Hrs expression vectors and STAM1 expression plasmids. Hrs is shown in *green* (Alexa 488), and STAM1 is shown in *red* (Alexa 594). Images taken with a longer exposure (*LE*) for *e* and *k* are shown in *e'* and *k'*. *Bars* indicate 20 μm.

when HRSd cells were transfected with STAM1 and ubiquitin, only faint STAM1 labeling was observed (Fig. 6*B*, *a*). In contrast, the co-introduction of wild-type Hrs and STAM1 resulted in the colocalization of these proteins (Fig. 6*B*, *d*, *e*, and *g*). Interestingly, heavy staining of ubiquitinated proteins overlapped with the staining of the STAM1·Hrs complex (Fig. 6*B*, *f* and *g*). Surprisingly, the introduction of Hrs-mUIM and STAM1 into HRSd cells induced enlarged endosomes in which the Hrs-mUIM and STAM1 immunoreactivity overlapped that of the ubiquitins (Fig. 6*B*, *h–k*).

Next, we examined whether the UIM of STAM1 played a role in the endosomal localization of these proteins and/or the endosomal phenotypes. When HRSd cells were transfected with STAM1-mUIM and ubiquitin, a slightly but significantly stronger signal for the STAM1-mUIM than for wild-type STAM1 was detected in the cytoplasm with a marginal increase in cytoplasmic ubiquitin expression (Fig. 6*B*, *l–l'*). In the presence of wild-type Hrs, the expression of STAM1-mUIM resulted in almost normal-sized endosomes that were co-localized with ubiquitins (Fig. 6*B*, *o–r*). However, when both STAM1 and Hrs were mutated at their UIM domains the HRSd cells clearly showed enlarged vesicles that co-localized with ubiquitins (Fig. 6*B*, *s–v*). These results suggest that Hrs and STAM1 co-localized with ubiquitinated proteins, and the intact UIM domain of Hrs but not of STAM1 is required for normal endosomal development. Collectively, these results suggest that Hrs is indispensable for the intracellular accumulation and endosomal localization of ubiquitins.

The UIM Domain of Hrs Is Essential for Enlarged Endosome Formation—Enlarged endosomes in the absence of Hrs have been reported (31, 32). We also examined the phenotypes of early endosomes in HRSd sublines expressing wild-type Hrs or its mutants using the co-expression of an endosomal marker protein, Eps15. By fluorescence microscopy, a scattered dot-like expression pattern of Eps15 was observed within the cytoplasm of HRSw cells that corresponded to the normal early endosome size and structure (Fig. 7*A*, *a*). In contrast, HRSd cells contained enlarged endosomes (Fig. 7*A*, *e*), and the two Hrs mutant cell lines Hrs-dC2 and -dFYVE exhibited a significantly enlarged endosome phenotype; the endosomes in these mutants were, however, smaller than those observed in HRSd cells (Fig. 7*A*, *b* and *c*). Cells expressing the Hrs mutant HRSdM, which fails to interact with either STAM1 or STAM2, also manifested modestly enlarged endosomes that lacked central transparency (Fig. 7*A*, *d*). Unexpectedly, the transient introduction of the Hrs-mUIM mutant also conferred an enlarged endosome phenotype (Fig. 7*B*, *m*). Thus, enlarged endosomes were observed in the absence of Hrs and in the presence of the Hrs-dC2, -dFYVE, -dM, and -mUIM mutants.

We next asked whether the subcellular localization of STAMs was altered in the presence or absence of wild-type or mutant Hrs. To examine the localization of Hrs and STAM1, we introduced Hrs and its mutants along with the STAM1 expression vector into HRSd cells (Fig. 7*B*). Consistent with the data in Fig. 7*A*, spot-like cytoplasmic expression of the wild-type Hrs and STAM1 was observed with nearly complete co-localization (Fig. 7*B*, *a–c*). Similar results were obtained when the STAM2 expression vector was introduced into HRSd cells (data not shown). Strikingly, when the Hrs-dC2 and -dM mutants were introduced, the STAM1 and Hrs mutants localized independently; Hrs localized to the enlarged endosomes, whereas STAM1 was diffusely expressed throughout the cytoplasm (Fig. 7*B*, *d–f* and *j–l*). The STAM1 immunoreactivity was significantly reduced when STAM1 was co-introduced with the Hrs-dC2 and Hrs-dM mutants but not with wild-type Hrs (Fig. 7*B*, *e* and *k*). Only long exposure images clearly showed the localization of STAM1 in the cytoplasm in the presence of these mutants (Fig. 7*B*, *e'* and *k'*). Interestingly, the Hrs-dFYVE mutant completely colocalized with STAM1, although the endosomes were enlarged and differed significantly from those seen with wild-type Hrs (Fig. 7*B*, *g–i*). These results indicate that the endosomal localization of STAM1 was dependent on its ability to bind Hrs because when it was cotransfected with Hrs mutants lacking STAM1 binding capability (HRSdC2 and HRSdM), STAM1 was expressed diffusely in the cytoplasm.

DISCUSSION

Stability of STAMs Is Dependent on Hrs—In this study we established an Hrs-deficient cell line and demonstrated the critical involvement of Hrs in the stability of both the STAM1 and STAM2 proteins. Whereas the Hrs-deficient HRSd cells showed a profound decrease in the level of STAM1 and STAM2, the stable introduction of Hrs fully restored both proteins to levels similar to those in normal MEFw cells. The drastic reduction in STAM1 and STAM2 could have been due to several possible factors, which are decreased transcription or translation, the stability of the mRNAs, or decreased protein stability. Our Northern blot analyses clearly demonstrated that the amount of STAM1 and STAM2 mRNA remained unchanged irrespective of the presence or absence of Hrs, indicating that instability of the STAM proteins accounted for the reduced levels. Similarly, transient transfection of the HRSd cells showed that the stability of both STAM1 and STAM2 was impaired. We, therefore, conclude that Hrs deficiency is likely to cause the STAM1 and STAM2 proteins to be unstable, and both proteins are therefore rapidly degraded so as to be undetectable on our regular Western blots.

Previous work by us indicated that both STAM1 and STAM2 firmly associate with Hrs through the CC2 domain of Hrs and the ITAM motif of STAM1 and STAM2 (4). Hrs probably binds the STAMs at a ratio of one to one, given that we observed only STAM1-Hrs and STAM2-Hrs heterodimeric complexes, but not a STAM1, STAM2, and Hrs trimeric complex (32). Here, neither STAM1 nor STAM2 was detected in HRSdC2 or HRSdM

cells, suggesting that the region containing the CC2 domain (amino acid 348–573) is necessary for the stability of the STAMs. Since the STAM proteins were detected in the Hrs-dFYVE mutant cell line, the FYVE domain of Hrs, which is required for Hrs to bind the inner surface of the cytoplasmic membrane through phosphatidylinositol 3,4,5-trisphosphate, is not necessary for the stability of the STAMs. The expression levels of Hrs in the Hrs-dC2 and Hrs-dM mutant cell lines, however, were markedly reduced and accompanied by the loss of STAM1 and STAM2. These results suggest that Hrs stabilizes the STAMs by directly binding to them.

The ITAM domain of STAM1 and STAM2 is required for binding to Hrs, although an additional region, called the SSM domain (in human STAM1, amino acids 297–320 and human STAM2 amino acids 286–309) may possess auxiliary Hrs binding functions (36). Given that the Hrs-dC2 mutation resulted in the degradation of STAM1, we expected the STAM1-DIT mutant, which is incapable of binding to Hrs, to be unstable. Consistent with this, the degradation of the STAM1-DIT mutant was significantly faster than that of wild-type STAM1. Our previous report using STAM1/STAM2 double-deficient cells clearly demonstrated that Hrs protein degradation is not controlled by the STAMs (32). Furthermore, a recent report showed that an Hrs knockdown induces Tsg101 instability, suggesting that Hrs also helps stabilize Tsg101. Since Tsg101 was recently shown to interact with Hrs and is now categorized as an ESCRT-I molecule, Hrs may function to stabilize other proteins as well (37). Taken together, our results show that STAM1 is stabilized by an association with Hrs, and Hrs mutants that disrupt STAM1 binding result in STAM1 degradation.

How does the deficiency of Hrs mediate STAM1 and STAM2 protein stability? In general, there are two major protein degradation systems, the ubiquitin-proteasome and the lysosome/vacuole pathways. These two pathways seem to regulate protein fate differentially, so that proteins with short half-lives tend to be degraded by the ubiquitin-proteasome pathway, whereas those with long half-lives are more likely to be digested by the lysosome/vacuole pathway (35). Our present results clearly indicated that the STAM1 degradation was proteasome-dependent. This was unexpected, because both STAMs and Hrs were previously shown to be resident endosomal proteins and believed to function in the endosome maturation machinery. A possible scenario, taken from recent data, is that the ESCRT complex could mediate protein degradation through a vesicular transport function (1). In this hypothesis protein ubiquitination has an indispensable function for transport. According to our present data, as long as Hrs is present ubiquitinated proteins can accumulate within the endosomes. Since the STAMs can hardly be detected in the absence of Hrs, we cannot fully exclude the possibility that STAM1 plays a role in the accumulation of ubiquitinated proteins within endosomes. Nevertheless, our data provide further evidence supporting the idea that ESCRT proteins mediate the accumulation of ubiquitinated proteins into endosomes, where the proteins are destined to be degraded in a lysosome-dependent manner.

Both the STAMs and Hrs possess a UIM domain, which was first identified as a polyubiquitin-binding site in the S5a subunit of the 26 S proteasome (38). The results of our mutational analysis suggest that the UIM domain of Hrs is not involved in the degradation of STAM1. However, the UIM domain of STAM1 is essential for its stability. A STAM1 mutant with point mutations within the UIM (STAM1-mUIM) was significantly more stable than wild-type STAM1 (STAM1-UIM), indicating that STAM1 controls its own degradation by the proteasome pathway. At present we have at least three hypotheses to explain the STAM1-UIM function. First, the UIM of STAM1 may contain one or more major polyubiquitinated sites. The UIM domain of STAM1 contains three lysine residues (Lys-171, Lys-178, and Lys-185) that are potentially polyubiquitinated and destined to be recognized by the 26 S proteasome for degradation. Indeed, of the three lysine residues, the first two are evolutionarily conserved from *Drosophila* to human. Although lysine 171 is a potential protein modification site for both ubiquitination and sumoylation, it is unlikely to play an important role in this degradation, since our UIM mutant conserves all three lysine residues (39). Second, the UIM domain of STAM1 may interact with other polyubiquitinated proteins, which will be recognized and degraded by the proteasome. However, it is unknown whether the degradation of any given protein can be mediated via interactions with another ubiquitinated protein(s). Recently, Hrs was shown to interact with AIP4, a HECT domain-containing E3 ubiquitin ligase (40). We, therefore, propose a third mechanism whereby the UIM domain of STAM1 interacts with an E3 enzyme(s) either alone or as a complex and, thus, allows STAMs to be ubiquitinated and thereby destined for degradation. Hrs is ubiquitinated by AIP4 and mediates the sorting of chemokine receptor CXCR4 into endosomes (40). In agreement with this, we also detected a significant increase in the level of the Hrs-mUIM protein compared with wild-type Hrs, suggesting its stabilization through the UIM via interactions with one or more ubiquitinase enzymes. We provide direct evidence that the UIM domain of Hrs (or some other UIM-interaction protein(s)) is not required for STAM1 degradation. To further analyze the mechanism underlying the degradation of STAMs, it will be necessary to identify an E3 enzyme that couples with the STAMs.

Hrs Causes Accumulation of Ubiquitinated Proteins—Previous studies have shown that the UIM domains of mammalian Hrs and yeast Vps27 are both essential for sorting ubiquitinated membrane proteins into the degradation pathway (2, 12, 41). Consistent with this, Hrs binds to monoubiquitinated proteins through its UIM domain (2, 12, 41). However, little is known about the role Hrs plays in intracellular polyubiquitination. The introduction of Hrs into HRSd cells caused the marked elevation of ubiquitinated proteins irrespective of the presence of STAM1 expression vectors. At present, the mechanism underlying the ubiquitinated protein accumulation is unclear. It is clear that the aberrantly enlarged endosomes do not account for the ubiquitin accumulation within whole-cell extracts because the class E compartment does not show any accumulation of ubiquitinated proteins in the absence of Hrs but, rather, manifests a significant decrease in ubiquitinated proteins. One possible explanation is that Hrs may control the activity of an E3 ubiquitin ligase. Cargo proteins captured by Hrs could be stabilized and/or further receive ubiquitination, probably through E3 group ubiquitinases within the Hrs complex. However, since the Hrs-mUIM mutant showed only a marginal decrease in intracellular ubiquitination, it may be that other E3 ligases are involved in ubiquitin accumulation. Since STAM1, STAM2, and Tsg101, which all belong to the ESCRT complex, possess additional ubiquitin-binding motifs, ESCRT molecules including Hrs may function as a complex to increase protein ubiquitination and/or protein stabilization. Conversely, our present data suggest that at least some ubiquitinated proteins accumulate within the endosomes. Therefore, ubiquitinated proteins destined to be degraded by the late endosome/lysosome system may be modified by Hrs. Interestingly, the overexpression of STAM2 in the presence of Hrs was recently reported to significantly increase the levels of intracellular ubiquitinated

proteins (36, 42). Our present data using Hrs-defective cells clearly indicate that the overexpression of STAM1 does not lead to an increase in ubiquitinated proteins. This difference might be due to the effects of excessive amounts of STAM2 and/or the presence of native Hrs in their experiment. Although further experiments are needed to clarify the mechanism, we propose that dysregulation of the STAM·Hrs complex may affect intracellular ubiquitination accumulation and the degradation machinery.

Enlarged Endosome Phenotype Is Dependent on Hrs—Recent studies by us (32) and others (19, 42) have provided evidence that the STAMs and Hrs co-localize in early endosomes. An earlier report demonstrated that Hrs can be co-immunoprecipitated with Eps15, an endosomal marker protein (43). Hrs has also been shown to bind Eps15 through the N-terminal half of Hrs (44). The direct binding of STAM1 with Eps15 was also reported (43). Since Eps15, an early endosomal membrane protein, is involved in the endocytosis of membrane-associated receptors via its binding to AP-2 (45), both the STAMs and Hrs are also localized to the same vesicles.

The lack of Hrs triggers aberrant intracellular vesicle formation called class E compartments. This was first demonstrated in genetic analyses with yeast mutants manifesting similar large vesicular compartments (2). In this report, we also clearly demonstrated abnormally enlarged endosomes. This "mammalian class E compartment" was present in several Hrs mutants we tested that were introduced into HRSd cells. Although the degree of endosomal enlargement differed with the mutation, our present data suggest that the class E phenotype is dependent on the C-terminal, FYVE, or CC2 domain. We therefore speculate that intact Hrs is required for endosomes to have a normal appearance. Interestingly, a point mutation (L265E) within the UIM domain of Hrs abrogates the normal endosomal architecture. It is possible that an unidentified UIM interaction molecule(s) functions in the normal endosomal phenotype. Unlike the UIM of Hrs, point mutations within the UIM of STAM1 did not result in enlarged endosomes. The class E compartment phenotype can be determined, therefore, by the UIM domain of Hrs but not by that of the STAMs. It is of note that Hrs not only supported the protein stability of STAMs but also determined their intracellular localization; the absence of Hrs totally changed the localization of STAMs from the endosomes to the cytoplasm. On the other hand, Hrs, whether wild type or mutated, always localized to the endosomes. To understand how this co-localization occurs, further work will be required to identify the region(s) within Hrs that is responsible for its localization.

In Vivo Function of Hrs—We provide further evidence that Hrs is required for normal mouse development. Although our attempt to establish a conditional targeting mouse has been unsuccessful, probably because of the impaired function of the *"floxed"* exon 6, experiments using established cell lines carrying the null allele provided the unexpected finding that the Hrs knock-out leads to the functional extinction of the STAM1 and STAM2 proteins. Incidentally, the STAM1/STAM2 double-knock-out mice we have generated die *in utero* around E11.5, because the ventral fold fails to form.[2] It is not surprising that Hrs knock-out mice with no detectable STAM1 or STAM2 protein manifest an embryonic lethal phenotype as well (26, 31). Loss of Hrs and/or STAM function results in mammalian class E phenotypes, which are similar to the class E phenotypes of yeast Vps27 and Hse1. Paradoxically, an excess of Hrs protein seems to be toxic to cells, because the overexpression of Hrs leads to a similar enlargement of endosomes (13). These results suggest that the appropriate control of Hrs and STAM1/STAM2 may be critical for normal cell morphology and function. Given that Hrs is involved in the accumulation of intracellular ubiquitinated proteins, our next step should be to clarify the functional relationship between the ESCRT complex and the ubiquitination machinery.

[2] H. Kobayashi, N. Tanaka, S. Miura, and K. Sugamura, unpublished data.

REFERENCES

1. Raiborg, C., Rusten, T. E., and Stenmark, H. (2003) *Curr. Opin. Cell Biol.* **15**, 446–455
2. Bilodeau, P. S., Urbanowski, J. L., Winistorfer, S. C., and Piper, R. C. (2002) *Nat. Cell Biol.* **4**, 534–539
3. Takeshita, T., Arita, T., Asao, H., Tanaka, N., Higuchi, M., Kuroda, H., Kaneko, K., Munakata, H., Endo, Y., Fujita, T., and Sugamura, K. (1996) *Biochem. Biophys. Res. Commun.* **225**, 1035–1039
4. Asao, H., Sasaki, Y., Arita, T., Tanaka, N., Endo, K., Kasai, H., Takeshita, T., Endo, Y., Fujita, T., and Sugamura, K. (1997) *J. Biol. Chem.* **272**, 32785–32791
5. Endo, K., Takeshita, T., Kasai, H., Sasaki, Y., Tanaka, N., Asao, H., Kikuchi, K., Yamada, M., Chenb, M., O'Shea, J. J., and Sugamura, K. (2000) *FEBS Lett.* **477**, 55–61
6. Komada, M., and Kitamura, N. (1995) *Mol. Cell. Biol.* **15**, 6213–6221
7. Goodman, O. B., Jr., Krupnick, J. G., Gurevich, V. V., Benovic, J. L., and Keen, J. H. (1997) *J. Biol. Chem.* **272**, 15017–15022
8. Gaullier, J. M., Simonsen, A., D'Arrigo, A., Bremnes, B., Stenmark, H., and Aasland, R. (1998) *Nature* **394**, 432–433
9. Dell'Angelica, E. C., Klumperman, J., Stoorvogel, W., and Bonifacino, J. S. (1998) *Science* **280**, 431–434
10. ter Haar, E., Harrison, S. C., and Kirchhausen, T. (2000) *Proc. Natl. Acad. Sci. U. S. A.* **97**, 1096–1100
11. Raiborg, C., Bache, K. G., Mehlum, A., Stang, E., and Stenmark, H. (2001) *EMBO J.* **20**, 5008–5021
12. Raiborg, C., Bache, K. G., Gillooly, D. J., Madshus, I. H., Stang, E., and Stenmark, H. (2002) *Nat. Cell Biol.* **4**, 394–398
13. Komada, M., Masaki, R., Yamamoto, A., and Kitamura, N. (1997) *J. Biol. Chem.* **272**, 20538–20544
14. Chin, L. S., Raynor, M. C., Wei, X., Chen, H. Q., and Li, L. (2001) *J. Biol. Chem.* **276**, 7069–7078
15. Bishop, N., Horman, A., and Woodman, P. (2002) *J. Cell Biol.* **157**, 91–101
16. Takeshita, T., Arita, T., Higuchi, M., Asao, H., Endo, K., Kuroda, H., Tanaka, N., Murata, K., Ishii, N., and Sugamura, K. (1997) *Immunity* **6**, 449–457
17. Lohi, O., Poussu, A., Merilainen, J., Kellokumpu, S., Wasenius, V. M., and Lehto, V. P. (1998) *J. Biol. Chem.* **273**, 21408–21415
18. Pandey, A., Fernandez, M. M., Steen, H., Blagoev, B., Nielsen, M. M., Roche, S., Mann, M., and Lodish, H. F. (2000) *J. Biol. Chem.* **275**, 38633–38639
19. Bache, K. G., Raiborg, C., Mehlum, A., and Stenmark, H. (2003) *J. Biol. Chem.* **278**, 12513–12521
20. Nakai, S., Kawano, H., Yudate, T., Nishi, M., Kuno, J., Nagata, A., Jishage, K., Hamada, H., Fujii, H., and Kawamura, K. (1995) *Genes Dev.* **9**, 3109–3121
21. Schonemann, M. D., Ryan, A. K., McEvilly, R. J., O'Connell, S. M., Arias, C. A., Kalla, K. A., Li, P., Sawchenko, P. E., and Rosenfeld, M. G. (1995) *Genes Dev.* **9**, 3122–3135
22. Bermingham, J. R., Jr., Scherer, S. S., O'Connell, S., Arroyo, E., Kalla, K. A., Powell, F. L., and Rosenfeld, M. G. (1996) *Genes Dev.* **10**, 1751–1762
23. Imamoto, A., and Soriano, P. (1993) *Cell* **73**, 1117–1124
24. Tanaka, N., Kamanaka, M., Enslen, H., Dong, C., Wysk, M., Davis, R. J., and Flavell, R. A. (2002) *EMBO Rep.* **3**, 785–791
25. Niwa, H., Yamamura, K., and Miyazaki, J. (1991) *Gene (Amst.)* **108**, 193–199
26. Miura, S., Takeshita, T., Asao, H., Kimura, Y., Murata, K., Sasaki, Y., Hanai, J. I., Beppu, H., Tsukazaki, T., Wrana, J. L., Miyazono, K., and Sugamura, K. (2000) *Mol. Cell. Biol.* **20**, 9346–9355
27. Polo, S., Sigismund, S., Faretta, M., Guidi, M., Capua, M. R., Bossi, G., Chen, H., De Camilli, P., and Di Fiore, P. P. (2002) *Nature* **416**, 451–455
28. Ebisawa, T., Fukuchi, M., Murakami, G., Chiba, T., Tanaka, K., Imamura, T., and Miyazono, K. (2001) *J. Biol. Chem.* **276**, 12477–12480
29. Yamada, M., Takeshita, T., Miura, S., Murata, K., Kimura, Y., Ishii, N., Nose, M., Sakagami, H., Kondo, H., Tashiro, F., Miyazaki, J. I., Sasaki, H., and Sugamura, K. (2001) *Mol. Cell. Biol.* **21**, 3807–3819
30. Yamada, M., Ishii, N., Asao, H., Murata, K., Kanazawa, C., Sasaki, H., and Sugamura, K. (2002) *Mol. Cell. Biol.* **22**, 8648–8658
31. Komada, M., and Soriano, P. (1999) *Genes Dev.* **13**, 1475–1485
32. Kanazawa, C., Morita, E., Yamada, M., Ishii, N., Miura, S., Asao, H., Yoshimori, T., and Sugamura, K. (2003) *Biochem. Biophys. Res. Commun.* **309**, 848–856
33. van Kerkhof, P., Alves dos Santos, C. M., Sachse, M., Klumperman, J., Bu, G., and Strous, G. J. (2001) *Mol. Biol. Cell* **12**, 2556–2566
34. Koinuma, D., Shinozaki, M., Komuro, A., Goto, K., Saitoh, M., Hanyu, A., Ebina, M., Nukiwa, T., Miyazawa, K., Imamura, T., and Miyazono, K. (2003) *EMBO J.* **22**, 6458–6470
35. Onodera, J., and Ohsumi, Y. (2004) *J. Biol. Chem.* **279**, 16071–16076
36. Mizuno, E., Kawahata, K., Okamoto, A., Kitamura, N., and Komada, M. (2004) *J. Biochem. (Tokyo)* **135**, 385–396
37. Bache, K. G., Brech, A., Mehlum, A., and Stenmark, H. (2003) *J. Cell Biol.* **162**, 435–442
38. Young, P., Deveraux, Q., Beal, R. E., Pickart, C. M., and Rechsteiner, M. (1998) *J. Biol. Chem.* **273**, 5461–5467
39. Sampson, D. A., Wang, M., and Matunis, M. J. (2001) *J. Biol. Chem.* **276**, 21664–21669

40. Marchese, A., Raiborg, C., Santini, F., Keen, J. H., Stenmark, H., and Benovic, J. L. (2003) *Dev. Cell* **5**, 709–722
41. Shih, S. C., Katzmann, D. J., Schnell, J. D., Sutanto, M., Emr, S. D., and Hicke, L. (2002) *Nat. Cell Biol.* **4**, 389–393
42. Mizuno, E., Kawahata, K., Kato, M., Kitamura, N., and Komada, M. (2003) *Mol. Biol. Cell* **14**, 3675–3689
43. Hansen, K., Ronnstrand, L., Claesson-Welsh, L., and Heldin, C. H. (1997) *FEBS Lett.* **409**, 195–200
44. Bean, A. J., Davanger, S., Chou, M. F., Gerhardt, B., Tsujimoto, S., and Chang, Y. (2000) *J. Biol. Chem.* **275**, 15271–15278
45. van Delft, S., Schumacher, C., Hage, W., Verkleij, A. J., and van Bergen en Henegouwen, P. M. (1997) *J. Cell Biol.* **136**, 811–821

Available online at www.sciencedirect.com
SCIENCE DIRECT®
Biochemical and Biophysical Research Communications 320 (2004) 18–26
BBRC
www.elsevier.com/locate/ybbrc

Nuclear trafficking of macromolecules by an oligopeptide derived from Vpr of human immunodeficiency virus type-1

Takashi Taguchi,[a] Mari Shimura,[a] Yoshiaki Osawa,[a] Yasunori Suzuki,[a] Izuru Mizoguchi,[a] Koitsu Niino,[b] Fumimaro Takaku,[c] and Yukihito Ishizaka[a,*]

[a] *Department of Intractable Diseases, International Medical Center of Japan, 1-21-1 Toyama, Shinjuku-ku, Tokyo 162-8655, Japan*
[b] *Niino Clinic, 1-64 Sakuragi-cho, Yonezawa, Yamagata 992-0027, Japan*
[c] *Jichi Medical School, 3311-1 Yakushiji, Minamikawachi-machi, Kawachi-gun, Tochigi 329-0498, Japan*

Received 12 March 2004
Available online 8 June 2004

Abstract

Vpr, an accessory gene product of HIV-1, is incorporated into cells when added to the culture medium. Via such function Vpr has been shown to transduce a protein into cells that is expressed as a chimeric protein with Vpr. The domain required for protein transduction, however, remained to be clarified. Here we identified a sequence encompassing 52–78 amino acids of Vpr (C45D18) that enables nuclear trafficking of proteins. When chemically synthesized C45D18 was added to the culture medium of human cord blood mononuclear (CBMN) cells, most cells became positive for the incorporated C45D18. Furthermore, recombinant proteins conjugated with the C45D18 were efficiently transduced and transported to regions corresponding to the nucleus. Incorporation of C45D18-conjugated protein was observed within a few hours after addition of the protein, independent of cellular growth. Although it is well known that Tat-derived peptide has a transducing activity, C45D18 was more active than Tat peptide for trafficking proteins into cells. Taking together with results from FACS analysis revealing that more than 90% of CBMN cells were positive for X-gal staining after treatment of C45D18-conjugated β-galactosidase, we propose that C45D18 translocates bioactive macromolecules directly into the nucleus.

Keywords: HIV-1; Vpr; Nuclear trafficking; Protein transduction domain; Resting cells

Vpr, one of six auxiliary genes of human immunodeficiency virus type 1 (HIV) [1,2] encodes a virion-associated protein [3–5], and has been proposed as a factor crucial for HIV-1 infection in resting macrophages [6]. Several lines of evidence indicate that Vpr is involved in translocation of preintegration complex from cytoplasm to nucleus [6,7]. Vpr is a small protein composed of 96 amino acids (aa), but has several functional domains of three α-helix regions (17–29, 36–47, and 53–78, respectively), a leucine-rich region from 60 to 80 aa, and C-terminal arginine-rich region [7]. It has been noted that Vpr has two separable parts responsible for nuclear translocation [8]. On the other hand, we previously reported that Vpr induces genomic instability by causing chromosome breaks and aneuploidy [9,10]. Our experiments also revealed that the C-terminal region of Vpr is important for cell-cycle arrest, and Vpr mutant lacking C-terminal 18 aa was negative for inducing cell-cycle abnormality at the G2/M phase.

As a particularly interesting property, Vpr functions like a transacting factor, and latently infected cells restart viral production, when Vpr is extracellularly added to cells [11,12]. In addition to such an activity, Vpr can enter cells when it is added to culture medium [7,13]. Consistently, a synthetic full-length peptide of Vpr or C-half of Vpr was used for efficient transduction of plasmid DNA [14]. On the other hand, Sherman et al. [15] recently reported that Vpr could transport exogenous proteins into cells. A fusion protein of Vpr with β-galactosidase (β-gal) was also shown to enter cells.

* Corresponding author. Fax: +81-3-5272-7527.
E-mail address: zakay@ri.imcj.go.jp (Y. Ishizaka).

0006-291X/$ - see front matter © 2004 Elsevier Inc. All rights reserved.
doi:10.1016/j.bbrc.2004.05.126

Such a transduction activity of Vpr is energy independent and does not require a cellular receptor [15]. As one of possibly related mechanisms of transducing activity, Vpr forms a channel in cellular membranes [16,17], and the amino-terminal region of 40 aa of Vpr with α-helix structures is responsible for the ion channel formation [17].

Proteins, such as antennapedia of *Drosophila* (ANTP) [18], VP22 of herpes simplex [19], and Tat of HIV-1 [20], are known to possess protein transduction domains (PTD). PTD enables proteins to cross biological membranes and helps them to enter the cytoplasm. It has been also reported that a variety of proteins, when expressed as chimetric proteins with the peptide, enter target cells. PTD has an arginine-rich region, and it was expected that the C-terminal region of Vpr, which contains an arginine-rich stretch, functioned as PTD. It was, however, concluded that the C-terminal half of Vpr did not show any activities as PTD [15], and the region of Vpr responsible for transducing exogenous protein remained to be clarified.

In the present study, we identified a sequence corresponding to the third α-helix domain (C45D18) as PTD. Interestingly, C45D18 entered cells even without cellular growth, and C45D18-conjugated green fluorescent protein (GFP) was quickly transferred to the nucleus. Transduction of protein conjugated with C45D18 was more efficient than that conjugated with Tat-derived peptide. Based on results that C45D18-conjugated proteins were efficiently transduced into cord blood mononuclear (CBMN) cells as well as resting adherent cells, we propose that C45D18 functions as a novel vehicle that facilitates nuclear trafficking of molecules into target cells.

Materials and methods

Cell culture and chemicals. HT1080 and HeLa cells were cultured in Dulbecco's modified Eagle's medium supplemented with 10% fetal calf serum (FCS) (Sigma, SI). Cord blood was kindly provided by volunteers who gave informed consent. CBMN cells were prepared by centrifugation, according to the manufacturer's protocol (Nycomed Pharma AS, Norway). Briefly, cord blood was diluted with the same amount of phosphate buffered saline (PBS) and applied on the Lymphoprep solution. After centrifugation for 20 min at 800g, cells at the interphase were collected, washed once with PBS, and resuspended in Iscove's modified Dulbecco's medium (IMDM) supplemented with 10% FCS. Jurkat cells and HL-60 cells were cultured in IMDM with 10% FCS. To prepare resting cells, HT1080 cells were cultured for 4 days in FCS-free medium. Cell growth of HL-60 cells was also arrested with 1 μg/ml aphidicolin (APC) (Sigma, SI). As a control, dimethyl sulfoxide (DMSO), used as a solvent of APC, was treated.

Peptide synthesis and detection of incorporated peptide. Various types of peptides derived from Vpr (see Fig. 1A) and Tat (GYGRKKRR QRRRGGC, amino acids described as single letters) were chemically synthesized (Wako, Tokyo). Biotin was added at the amino terminal end of each peptide. After treatment of peptides, cells were washed once with PBS and then fixed with 100% ice-cold methanol. To exclude signals associated with cellular membranes, cells were treated for 10 min with 0.2% Triton X-100 in PBS [21]. Cells were then reacted for 1 h with streptavidin (SA)-conjugated FITC (SA-FITC) and washed several times in PBS with 0.05% Tween 20. To detect the interaction of the peptide and plasmid DNA, different doses of the peptide (1–30 μg) were mixed with 0.2 μg plasmid DNA. A reporter plasmid, pCMV/luciferase, was kindly provided by Dr. Shimada (Nihon Medical School). Luciferase activity was assayed, as described [21].

Expression of recombinant green fluorescent protein and conjugation with peptides. A recombinant protein of green fluorescent protein (GFP) tagged with $(His)_6$ was expressed by a baculovirus system with pFASTBAC and purified with proband region (Invitrogen, Carlsbad, CA). Molecular weights of GFP and β-galactosidase (β-gal) (Wako, MI) were about 35 and 465 kDa, respectively. These proteins were chemically conjugated with Vpr-derived peptides (JBL, Fujioka, Japan). Briefly, about 300 μg protein was suspended in 10 mM phosphate buffer (pH 7.0) and added with 0.1 mM *N*-[e-maleimidocaproyloxiy]succinimide ester (DOJINDO Lab. Kumamoto, Japan). After 30 min at room temperature, each Vpr-derived peptide was added and further incubated for 3 h at room temperature. Conjugated molecules were then dialyzed against PBS overnight.

To test protein transduction, cells were incubated with conjugated proteins overnight and incorporated GFP was detected by an antibody. To demonstrate β-gal activity, X-gal staining was carried out according to the method described [22].

Fluorescent activated cell sorter (FACS) analysis. Incorporation of peptides was analyzed by detecting SA-FITC bound to the peptides. For cell-cycle analysis, cells were treated for 1 h with 10 μM bromodeoxyuridine (BrdU) (Sigma, St. Louis, MO). After fixation in 70% ice-cold ethanol, cells were treated with FITC-conjugated anti-BrdU antibody (Beckton–Dickinson, San Jose, CA) and then stained with 5 μM propidium iodide (Sigma). To study the effect of Vpr on cell-cycle, cells after treatment of peptides were stained with 50 μg/ml propidium iodide and subjected to FACS analysis. For FACS analysis of β-galactosidase activity, a FluoReporter lacZ Flow Cytometry Kit (Molecular Probes, Eugene, OR) was used. Briefly, 5×10^5/100 μl of CBMN cells was mixed with 1 mM fluorescein di-β-D-galactopyranoside for 1 min and was added to 1.8 ml of ice-cold PBS containing 1.5 μM propidium iodide. FACS analysis was carried out by Cellquest (Beckton–Dickinson, San Jose, CA).

Results

Identification of Vpr-derived oligopeptide with transducing activity

The carboxyl-half of Vpr has been shown to transduce plasmid DNA into cultured cells [14]. On the other hand, we previously reported that Vpr induced cell-cycle abnormality at the G2/M phase, but Vpr mutant that lacked C-terminal 18 amino acids was negative for the cell-cycle abnormality [9]. Based on these observations, we tested whether C-terminal 45 aa of Vpr without the extreme C-terminal 18 aa (C45D18, Fig. 1A) had a trafficking activity. A biotin-conjugated 27-mer peptide (52–78 aa) was synthesized, and 10 μg/ml of the peptide was added into the medium of cultured cells. On the next day, an incorporated peptide was detected with SA-FITC. As shown in Fig. 1B, C45D18 was clearly detected in the peptide-treated cells (Fig. 1B, middle

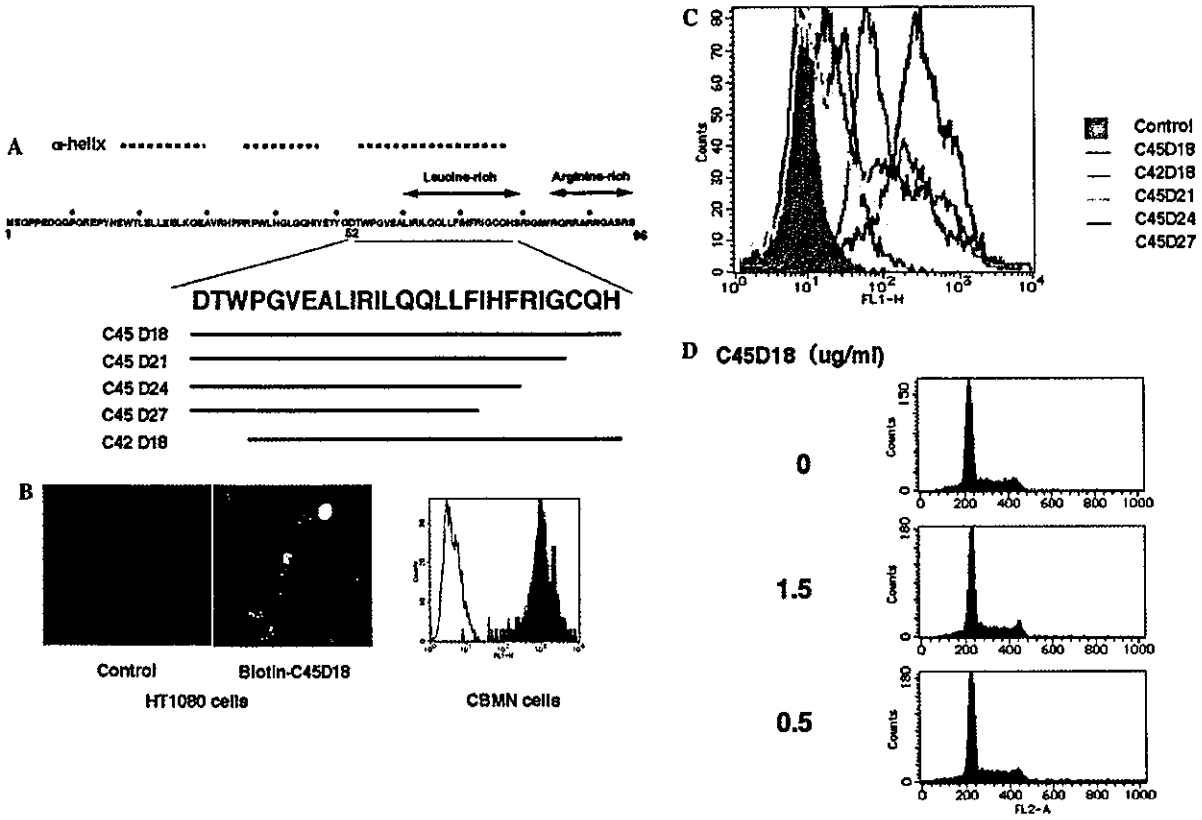

Fig. 1. Identification of Vpr-derived peptide that is incorporated into cells. (A) Amino acid sequence of Vpr used in the present study. (B) Incorporation of C45D18 into cells. Results of HT1080 cells (left panels) and CBMN cells (right panel) are shown. Note that almost all of cells are positive for the incorporated peptide (shown by yellow and red in left and right panels, respectively). (C) Transducing activity of synthetic peptides. Several biotin-conjugated peptides were synthesized and added into the culture medium of CBMN cells. On the next day, the incorporated peptides were detected with SA-FITC. Amino acid sequence of each peptide is shown in (A). (D) Effects of C45D18 on cell-cycle. Cells were treated with C45D18 for 2 days and then subjected to cell-cycle analysis. (For interpretation of the references to colour in this figure legend, the reader is referred to the web version of this paper.)

panel). We observed that C45D18 was also efficiently incorporated into CBMN cells (Fig. 1B, right panel shown by red). FACS analysis revealed that almost 100% of cells were positive for the incorporated peptide after overnight treatment.

To identify the minimal region required for such trafficking activity, several biotinylated peptides were synthesized (Fig. 1A), and we tested whether they were incorporated into CBMN cells, (Fig. 1C). Three peptides of C45D21 (52–75 aa), C45D24 (52–72 aa), and C45D27 (52–69 aa) were less efficiently incorporated to CBMN cells than C45D18 (orange, purple, and yellow peaks, respectively). When amino-terminal three amino acids were deleted from C45D18 (C42D18), its trafficking activity was greatly reduced (blue in Fig. 1C).

It has been reported that Vpr induces cell-cycle abnormality at G2/M phase, and we studied whether C45D18 has an activity on cell-cycle. As shown in Fig. 1D, FACS analysis revealed that cell-cycle was not changed after treatment for 2 days. These data imply that C45D18 is an appropriate sequence for further characterization of the potentiality for transducing activity.

Trafficking macromolecules

We next studied whether C45D18 could transduce plasmid DNA. Consistent with a previous report on the full-length peptide of Vpr [14], C45D18 interacted with plasmid DNA. Unfortunately, however, we could not obtain a favorable amount of exogenous gene expression in cells transfected with the complex (data not shown). To evaluate the activity of C45D18 to transport macromolecules into cells, we studied whether C45D18, when attached to a recombinant protein, entered cells. For this purpose, C45D18 was conjugated at various molar ratios with a purified recombinant protein of GFP and added into the culture medium. On the next day, incorporated proteins were detected. As shown in Fig. 2A, cells treated with C45D18-conjugated GFP were positive for incorporation, although the protein was not detected at all in cells treated with GFP by itself (Fig. 2A, left panel). In the present study, cells were treated with 0.2% Triton X-100 before treatment with SA-FITC. Since this procedure abolished signals associated with cellular membranes [21], our positive ob-

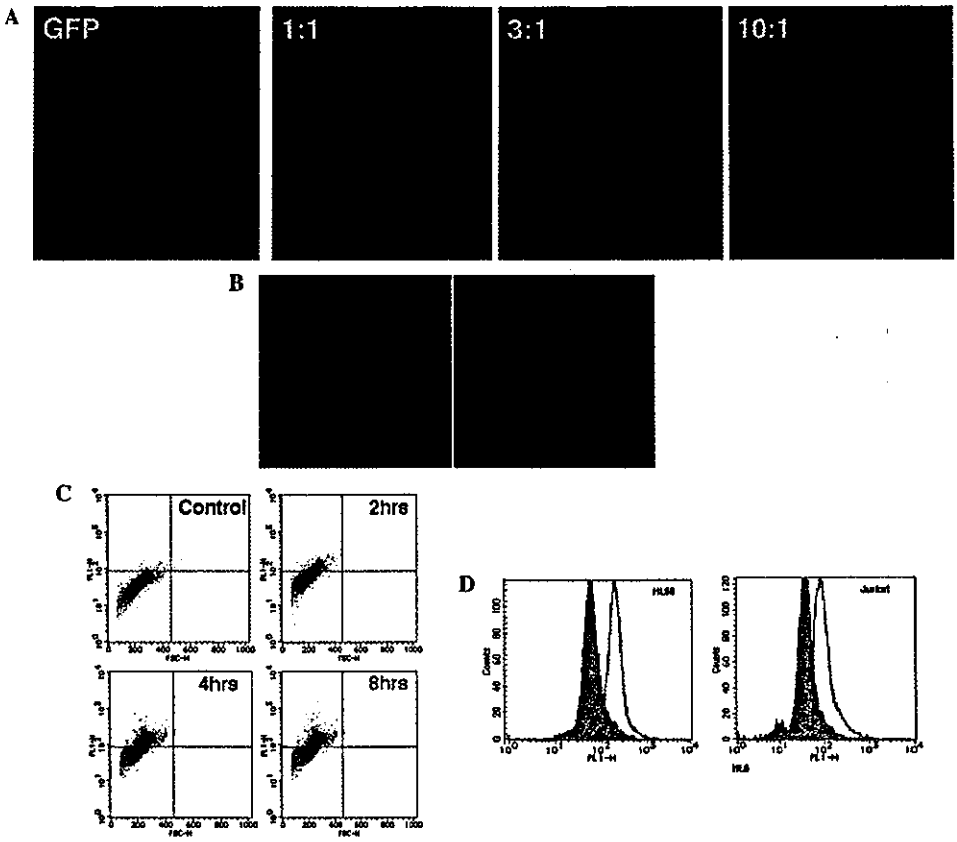

Fig. 2. Trafficking macromolecule by C45D18. (A) Incorporation of C45D18-conjugated GFP into HT1080 cells. GFP conjugated with different doses of C45D18 (3 μg/ml) was added to cells, and the incorporated GFP was detected by immunostaining with an antibody to GFP. The molar ratio of C45D18 to GFP was 1:1, 3:1, and 10:1. As a control just GFP (3 μg/ml) was added into the medium (left panel). (B) Nuclear localization of incorporated C45D18-conjugated GFP. GFP and nuclear DNA were stained with the antibody to GFP and Hoechst 33258. Incorporated GFP was detected by laser-scanning microscopy. Signals of GFP (left panel) and DNA (right panel) on the same field are shown by red and blue, respectively. (C) Time course of the incorporation of CV45D18-conjugated GFP. HL-60 cells were treated with C45D18-conjugated GFP (a molar ration of C45D18: GFP = 10:1) for 2 (upper right panel), 4 (lower left panel), and 8 h (lower right panel). As a control, cells were incubated with the conjugated GFP for 8 h. (D) Efficient trafficking by C45D18 compared to Tat-derived peptide. A chemically synthesized Tat-derived peptide (see Materials and methods) was conjugated to GFP according to the completely same procedures of C45D18, and added into culture medium of HL-60 (left panel) and Jurkat cells (right panel). Incorporated GFP, C45D18-GFP, and Tat-GFP were shown by red, orange, and blue, respectively. Note that C45D18-conjugated GFP was more efficiently incorporated than Tat-GFP. (For interpretation of the references to colour in this figure legend, the reader is referred to the web version of this paper.)

servations indicate that the C45D18-conjugated protein was actually incorporated into cells. The amount of incorporated proteins increased according to doses of C45D18 conjugated to the protein (Fig. 2A). As a further interesting observation, incorporated GFP was detected in the regions corresponding to the nuclei of treated cells. Laser-scanning microscopy clearly detected that the incorporated GFP was present in the nucleus (Fig. 2B, see also Fig. 3C), implying that C45D18 can be used for nuclear trafficking of macromolecules.

Characterization of C45D18-dependent trafficking of macromolecules

We characterized the C45D18-dependent incorporation of GFP. To accurately measure the population with incorporated GFP, HL-60 cells were treated with the C45D18-GFP (molar ratio = 10:1) and subjected to FACS analysis. First, the dose–response of the incorporation was studied. When cells were incubated with 6, 3, and 1.5 μg/ml of the conjugated protein, 70%, 50%, and 30% of cells were positive for the incorporated GFP, respectively (data not shown). The time-course analysis was next carried out using 3 μg/ml of the conjugated protein. The incorporation of peptide-conjugated GFP was observed within 2 h after treatment (Fig. 2B). About 30% of cells were positive for the protein (Fig. 2C, upper right panel). Then, about 50% of cells were positive for the incorporated GFP in 4 or 8 h (Fig. 2B, lower panels), indicating that most of the C45D18-dependent incorporation of conjugated protein was complete within several hours.

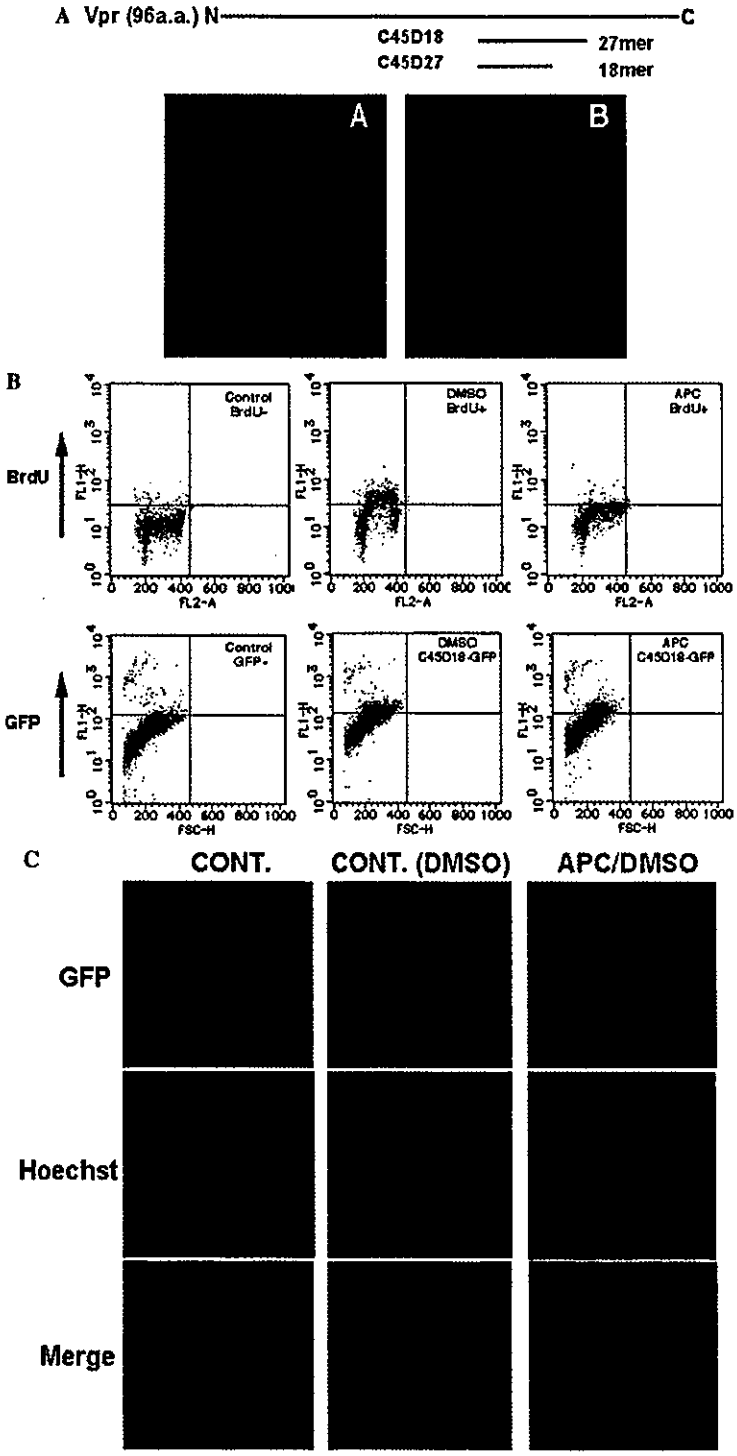

Fig. 3. Characterization of C45D18-dependent incorporation of GFP. (A) Incorporation of C45D18 into resting cells. HT1080 cells were arrested by serum-starvation for 4 days and then C45D18 or C47D27 was treated for about 12 h. Cell cycle arrest was confirmed by BrdU incorporation, followed by FACS analysis (data not shown). The incorporated peptides were detected with SA-FITC. Note that only C45D18 was incorporated into cells. (B) Incorporation of C45D18-conjugated GFP into resting cells. HL-60 cells were treated for 14 h with 1 μg/ml aphidicolin (APC), and then 3 μg/ml C45D18-conjugated GFP was treated for 5 h. Upper and lower panels show results of cell cycle analysis and incorporated GFP, respectively. As a control, cells were treated with DMSO, used as a solvent of APC (middle panels). After APC treatment, cells did not incorporate BrdU (upper right panel), but the incorporated GFP was detected in these cells (lower right panel). (C) Incorporation of C45D18-GFP into nucleus even under cell cycle arrest. HT1080 cells were treated for 14 h with 1 μg/ml APC and incubated with the conjugated GFP. The incorporated GFP was analyzed by laser-scanning microscopy. Results of C45D18-GFP added to control cells (left panels), DMSO-treated cells (middle panels), and APC-treated cells (right panels) are shown. Positive signals of the incorporated GFP (upper panels), DNA stained by Hoechst 33258 (middle panels), and merged images (lower panels) are shown.

It has been proposed that Tat, another accessory gene product of HIV-1, has a sequence of 9-mer aa with trafficking activity [20]. To compare the activity of C45D18 and Tat peptides, GFP was conjugated with each peptide at the same molar ratio (10:1) by the same procedure with C45D18. Then each protein was added to the culture media of two human cell lines, HL-60 and Jurkat cells. As shown in Fig. 2D, GFP conjugated with Tat peptide was not efficiently incorporated (blue), compared to the C45D18 (orange). In the present work, we conjugated peptides with protein through maleimide molecules and then directly added them to the culture medium without denaturing conjugated proteins. Since it is reported that Tat activity to transduce proteins is observed only after denaturing proteins [23], it may be possible that Tat activity of protein transduction is possibly detected after denaturing molecules.

It has been reported that Vpr has an activity to form channels in the cytoplasmic membrane [16,17], by which Vpr might be incorporated into cells. To exclude the possibility that trafficking of exogenous proteins is due to passive incorporation through membrane channels formed by Vpr-derived peptide, we added C45D18 and unconjugated GFP simultaneously, and then evaluated whether GFP was detected in the treated cells. No incorporated signals were observed (data not shown), indicating that C45D18 was active for transducing protein, only when it was conjugated with macromolecule.

Trafficking molecules into resting cells

It has been proposed that Vpr is responsible for infection of HIV to resting macrophages [6]. To know whether C45D18 could be incorporated into resting cells, HT1080 cells were first cultured for 4 days in FCS-free medium and then incubated with the peptide. FACS analysis on BrdU-positive cells clearly indicated that cells were not S-phase (data not shown). When C45D18 was treated with these cells, the peptide was again efficiently incorporated (Fig. 3A-A). By contrast, C45D28, a smaller peptide, was not incorporated at all (Figs. 3A and B), indicating that the incorporation of C45D18 was not due to the passive transport of small molecules into

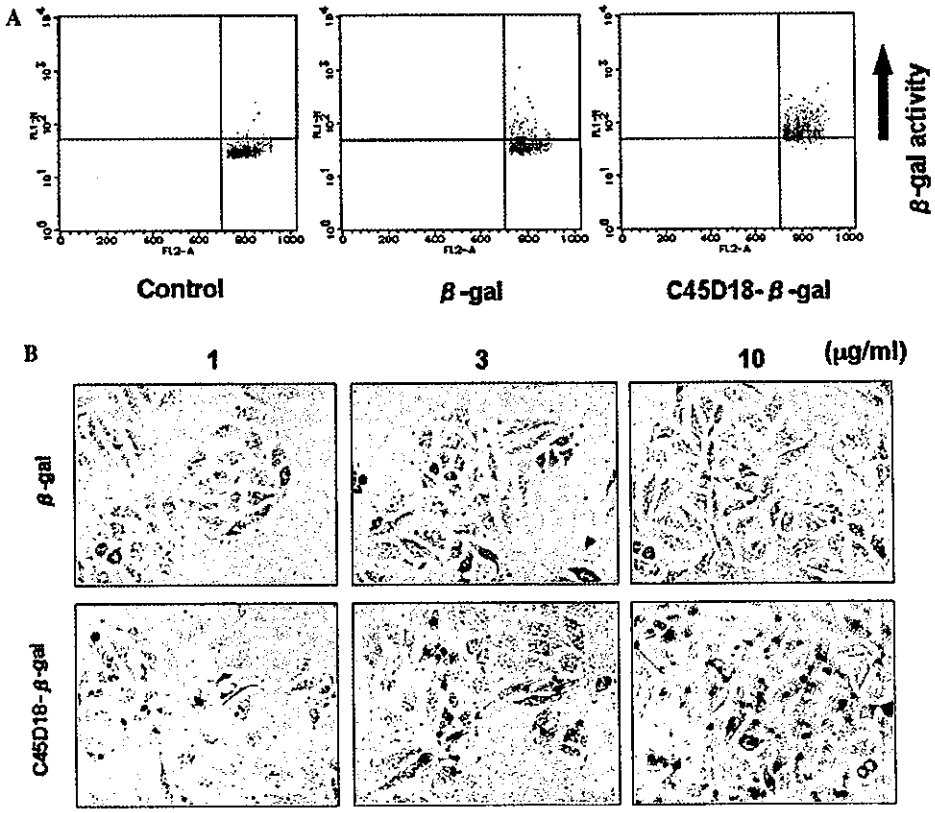

Fig. 4. Incorporation of bioactive molecule of C45D18. (A) Nuclear trafficking of active β-gal into adherent cells. HT1080 cells were treated overnight with control β-gal (upper panels) or C45D18-conjugated β-gal (lower panels). Then X-gal staining was carried out. Doses of treated proteins were 1 (left panels), 3 (middle panels), and 10 (right panels) μg/ml, respectively. β-Gal activity is indicated as black spots. Note that signals of β-gal activity are observed in regions corresponding to nucleus. (B) Incorporation of β-gal into CBMN cells by C45D18. CBMN cells were treated with C45D18-conjugated β-gal, and the activity of β-gal was detected by FACS analysis with a FluoReporter lacZ Flow Cytometry kit. Results of control (left panel), β-gal (middle panel), and β-gal conjugated with C45D18 (right panel) are shown.

cells. We next studied whether C45D18-conjugated protein was also incorporated into resting cells. HL-60 cells were first treated for 14 h with 1 μg/ml APC and then incubated for another 5 h with 3 μg/ml C45D18-conjugated GFP. We confirmed that cell cycle was completely arrested, as judged by incorporation of BrdU (Fig. 3B, upper right panel). Even under such condition, more than 50% of cells were positive for incorporated GFP (Fig. 3B, lower right panel). The same experiment was carried out on HT1080 cells and consistent results were obtained (Fig. 3C). Incorporation of C45D18-conjugated GFP into APC-treated cells was observed at almost the same level with control (Fig. 3D, right panels). Interestingly, the incorporated GFP was again detected in nuclear regions, judged by laser-scanning microscopy (Fig. 3C, middle and right panels). These data indicate that the nuclear trafficking of protein by C45D18 was not dependent on cellular growth.

Nuclear trafficking of bioactive macromolecules

To know whether C45D18 could transport a bioactive macromolecule, β-gal with a molecular weight of 465 kDa was conjugated with C45D18 and then added to cells. To show bioactivity, X-gal staining was carried out on the next day. As shown in Fig. 4A, β-gal activity was clearly detected in HT1080 cells treated with conjugated β-gal. The numbers of cells positive for of X-gal staining increased in a dose-dependent manner of treated β-gal (Fig. 4A). We also observed that β-gal activity was present in regions corresponding to nucleus.

C45D18-dependent incorporation of β-gal activity was also demonstrated by FACS analysis on CBMN cells that were treated with the protein (see Materials and methods). As shown in Fig. 4B, more than 90% of treated cells were positive for β-gal activity (Fig. 4B, right panel). By contrast, treatment of β-gal alone did not increase the number of cells positive for the activity (Fig. 4B, middle panel). These data indicate that the trafficking property by C45D18 can transduce bioactive molecule at high efficiency.

Discussion

In the present study, we identified a sequence encompassing 52–78 aa of Vpr (C45D18) as a novel PTD. To confirm the reproducibility of our observations, we synthesized C45D18 more than three times and examined the activity of the peptide conjugated with proteins. Independent experiments revealed that C45D18 or its conjugated proteins, when added to culture medium of cells, were efficiently incorporated into the nuclear region.

For nuclear trafficking of proteins into cells from outside, there are at least two steps where C45D18 should function. One is that C45D18 enables conjugated proteins to cross biomembranes, and another step is that C45D18 translocates the incorporated protein to the nucleus. Although the precise mechanism remains to be clarified, it has been well proposed that Vpr enters cells [7,13], when added to the culture medium. As a possible explanation of this phenomenon, it has been proposed that Vpr forms ion channels in cellular membranes [16,17]. The region responsible for channel formation has been recognized in amino-terminal 40 aa [17]. Crossing cellular membranes by the C45D18 would not, however, be due to the ion channel formation by a proposed region, since C45D18 is located in the C-terminal half of Vpr. How the conjugated protein enters cells remains to be clarified.

As one of the most important functions of Vpr, it is involved in the nuclear trafficking of a pre-integration complex of HIV-1 (PIC) [6,24], which explains an intriguing activity of HIV-1 to infect resting macrophages [25]. The mechanism of nuclear trafficking activity of Vpr has been extensively investigated, and it is well proposed that Vpr is a nucleopheric protein [6,24,26–28]. Interestingly, however, it does not have a classical nuclear localization signal. Although there are some controversial reports [8], it has been proposed that Vpr binds karyopherin α [6,24] and translocates PIC to the nucleus. Furthermore, Vpr has been shown to interact with members of nuclear pore complex (NPC) proteins such as Nsp1p [27] and nucleoporin hCG1 [28]. Functional analysis using chimeric proteins of Vpr and β-gal has indicated that two parts of Vpr promote nuclear trafficking of β-gal. It was reported that 71–96 aa of Vpr is still active in nuclear localization. Since C45D18 has a region of 53–78 aa, it might be possible that an overlapped region of 71–78 aa has an affinity to NPC proteins, responsible for nuclear trafficking. To know whether the overlapped region 71–78 aa of Vpr (peptide-8) functions for nuclear trafficking of C45D18, we added peptide-8 into culture medium of cells and compared with the properties of C45D18. Although we observed that C45D18 was incorporated into the nuclear region, but peptide-8 was scarcely translocated to nucleus (data not shown), implying that the region of 71–78 aa of Vpr is not enough for nuclear translocation of C45D18.

As an important observation, C45D18 could transduce exogenous molecules into resting cells. Although retrovirus gene transfer is frequently utilized in clinical fields, exogenous genes cannot be transduced in resting cells by the system. To circumvent this problem, modified lentiviral vectors are developed for transducing genes into resting cells [29]. On the other hand, recent observations reveal that a retroviral system occasionally results in fatal side effects [30], implying that a non-viral gene transfer system would be more reliable in future clinical use. In most of gene transfer systems, however, the expression of exogenous genes depends on break

down of nuclear membranes. To obtain an efficient gene expression in resting cells, it is crucial to develop a system by which exogenous genes are directly transferred into nucleus. Since C45D18 can efficiently translocate into the nucleus, it is tempting to speculate that the frequency of gene expression by non-viral gene transfer systems may be improved by the combination with C45D18.

It has been reported that several peptides derived from different sources—such as ANTP, herpes simplex VP22, and nine amino acids of Tat peptide-possess protein transduction activity. When compared to the activity of Tat, C45D18 has more potent activity in transporting molecules. It has been well proposed that the transduction activity of Tat requires protein denaturing [23]. Our present work reveals that C45D18 is more versatile than Tat peptide, since C45D18-conjugated molecules can be directly utilized for nuclear trafficking without any subsequent procedures. Additionally, C45D18 did not induce any cell-cycle abnormality or apoptosis (Fig. 1D), implying that it can be used without serious side effects.

Acknowledgments

We are grateful to Dr. Dovie Wylie for kind help with manuscript preparation. We also would like to express great thanks to IBL for technical help in conjugation of C45D18 and proteins. This work was supported by a Grant-in-Aid for Research on Human Genome, Tissue Engineering from the Ministries of Health, Labour and Welfare of Japan. This work was also partly supported by a research grant from the Rinsho Yakuri Research Foundation. Yoshiaki Osawa is a research resident supported by the Japanese Foundation for AIDS Prevention.

References

[1] F. Wong-Staal, P.K. Chanda, J. Ghrayeb, Human immunodeficiency virus: the eighth gene, AIDS Res. Hum. Retroviruses 3 (1987) 33–39.
[2] E.A. Cohen, R.A. Subbramanian, H.G. Göttlinger, Role of auxiliary proteins in retroviral morphogenesis, Curr. Top. Microbiol. Immunol. 214 (1996) 219–235.
[3] X.F. Yu, M. Matsuda, M. Essex, T.H. Lee, Open reading frame *vpr* of simian immunodeficiency virus encodes a virion-associated protein, J. Virol. 64 (1990) 5688–5693.
[4] W. Paxton, R.I. Connor, N.R. Landau, Incorporation of vpr into human immunodeficiency virus type 1 virions: requirement for the p6 region of *gag* and mutational analysis, J. Virol. 67 (1993) 7229–7237.
[5] E.A. Cohen, G. Dehni, J.G. Sodroski, W.A. Haseltine, Human immunodeficiency virus *vpr* product is a virion-associated regulatory protein, J. Virol. 64 (1990) 3097–3099.
[6] M.A. Vodicka, D.M. Koepp, P.A. Silver, M. Emerman, HIV-1 Vpr interacts with the nuclear transport pathway to promote macrophage infection, Genes Dev. 12 (1998) 175–185.
[7] P. Henklein, K. Bruns, M.P. Sherman, U. Tessmer, K. Licha, J. Kopp, C.M.C. de Noronha, W.C. Greene, V. Wray, U. Schubert, Functional and structural characterization of synthetic HIV-1 Vpr that transduces cells, localizes to the nucleus, and induces G2 cell cycle arrest, J. Biol. Chem. 275 (2000) 32016–32026.
[8] Y. Jenkins, M. McEntee, K. Weis, W.C. Greene, Characterization of HIV-1 vpr nuclear import: analysis of signals and pathways, J. Cell Biol. 143 (1998) 875–885.
[9] M. Shimura, Y. Tanaka, S. Nakamura, Y. Minemoto, K. Yamashita, K. Hatake, F. Takaku, Y. Ishizaka, Micronuclei formation and aneuploidy induced by Vpr, an accessory gene of human immunodeficiency virus type 1, FASEB J. 13 (1999) 621–637.
[10] M. Shimura, Y. Onozuka, T. Yamaguchi, K. Hatake, F. Takaku, Y. Ishizaka, Micronuclei formation with chromosome breaks and gene amplification caused by Vpr, an accessory gene of human immunodeficiency virus, Cancer Res. 59 (1999) 2259–2264.
[11] D.N. Levy, Y. Refaeli, R.R. MacGregor, D.B. Weiner, Serum Vpr regulates productive infection and latency of human immunodeficiency virus type 1, Proc. Natl. Acad. Sci. USA 91 (1994) 10873–10877.
[12] D.N. Levy, Y. Refaeli, D.B. Weiner, Extracellular Vpr protein increases cellular permissiveness to human immunodeficiency virus replication and reactivates virus from latency, J. Virol. 69 (1995) 1243–1252.
[13] M.-B. Huang, O. Weeks, L.-J. Zhao, M. Saltarelli, V.C. Bond, Effects of extracellular human immunodeficiency virus type 1 vpr protein in primary rat cortical cell cultures, J. Neurovirol. 6 (2000) 202–220.
[14] A. Kichler, J.C. Pages, C. Leborgne, S. Druillennec, C. Lenoir, D. Coulaud, E. Delain, E. Le Cam, B.P. Roques, O. Danos, Efficient DNA transfection mediated by the C-terminal domain of human immunodeficiency virus type 1 viral protein R, J. Virol. 74 (2000) 5424–5431.
[15] M.P. Sherman, U. Schubert, S.A. Williams, C.M.C. de Noronha, J.F. Kreisberg, P. Henklein, W.C. Greene, HIV-1 Vpr displays natural protein-transducing properties: implications for viral pathogenesis, Virology 302 (2002) 95–105.
[16] S.C. Piller, G.D. Ewart, A. Premkumar, G.B. Cox, P.W. Gage, Vpr protein of human immunodeficiency virus type 1 forms cation-selective channels in planar lipid bilayers, Proc. Natl. Acad. Sci. USA 93 (1996) 111–115.
[17] S.C. Piller, G.D. Ewart, D.A. Jans, P.W. Gage, G.B. Cox, The amino-terminal region of Vpr from human immunodeficiency virus type 1 forms ion channels and kills neurons, J. Virol. 73 (1999) 4230–4238.
[18] S. Console, C. Marty, C. Garcia-Echeverria, R. Schwendener, K. Ballmer-Hofer, Antennapedia and HIV transactivator of transcription (TAT) protein transduction domains promote endocytosis of high molecular weight cargo upon binding to cell surface glycosaminoglycans, J. Biol. Chem. 278 (2003) 35109–35114.
[19] G. Elliott, P. O'Hare, Intercellular trafficking and protein delivery by a herpesvirus structural protein, Cell 88 (1997) 223–233.
[20] N.J. Caron, Y. Torrente, G. Camirand, M. Bujold, P. Chapdelaine, K. Leriche, N. Bresolin, J.P. Tremblay, Intracellular delivery of a Tat-eGFP fusion protein into muscle cells, Mol. Ther. 3 (2001) 310–318.
[21] L. Yano, M. Shimura, M. Taniguchi, Y. Hayashi, T. Suzuki, K. Hatake, F. Takaku, Y. Ishizaka, Improved gene transfer to neuroblastoma cells by a monoclonal antibody targeting RET, a receptor tyrosine kinase, Hum. Gene Ther. 11 (2000) 995–1004.
[22] J. Sambrook, D.W. Russell, Molecular Cloning: A Laboratory Manual, Cold Spring Harbor Laboratory Press, Cold Spring Harbor, NY, 2001.
[23] M.C. Morris, J. Depollier, J. Mery, F. Heitz, G. Divita, A peptide carrier for the delivery of biologically active proteins into mammalian cells, Nat. Biotechnol. 19 (2001) 1173–1176.
[24] S. Popov, M. Rexach, G. Zybarth, N. Reiling, M.A. Lee, L. Ratner, C.M. Lane, M.S. Moore, G. Blobel, M. Bukrinsky, Viral protein R regulates nuclear import of the HIV-1 pre-integration complex, EMBO J. 17 (1998) 909–917.

[25] M.A. Vodicka, Determinants for lentiviral infection of non-dividing cells, Somat. Cell Mol. Genet. 26 (2001) 35–49.
[26] S. Popov, M. Rexach, L. Ratner, G. Blobel, M. Bukrinsky, Viral protein R regulates docking of the HIV-1 preintegration complex to the nuclear pore complex, J. Biol. Chem. 273 (1998) 13347–13352.
[27] R.A.M. Fouchier, B.E. Meyer, J.H.M. Simon, U. Fischer, A.V. Albright, F. Gonzalez-Scarano, M.H. Malim, Interaction of the human immunodeficiency virus type 1 Vpr protein with the nuclear pore complex, J. Virol. 72 (1998) 6004–6013.
[28] E. Le Rouzic, A. Mousnier, C. Rustum, F. Stutz, E. Hallberg, C. Dargemont, S. Benichou, Docking of HIV-1 Vpr to the nuclear envelope is mediated by the interaction with the nucleoporin hCG1, J. Biol. Chem. 277 (2002) 45091–45098.
[29] F. Galimi, I.M. Verma, Opportunities for the use of lentiviral vectors in human gene therapy, Curr. Top. Microbiol. Immunol. 261 (2002) 245–254.
[30] E. Marshall, Gene therapy. Second child in French trial is found to have leukemia, Science 299 (2003) 320.

Available online at www.sciencedirect.com
SCIENCE DIRECT®
Biochemical and Biophysical Research Communications 316 (2004) 226–232
BBRC
www.elsevier.com/locate/ybbrc

Nuclear export signal in CDC25B

Sanae Uchida,[a] Motoaki Ohtsubo,[b,1] Mari Shimura,[c] Masato Hirata,[d] Hitoshi Nakagama,[e] Tsukasa Matsunaga,[f] Minoru Yoshida,[g,h] Yukihito Ishizaka,[c] and Katsumi Yamashita[a,*]

[a] *Division of Life Science, Graduate School of Natural Science and Technology, Kanazawa University, General Education Hall, Kakuma-machi, Kanazawa 920-1192, Japan*
[b] *Institute of Life Science, Kurume University, Aikawa 2432-3, Kurume 839-0861, Japan*
[c] *Division of Intractable Disease, International Medical Center of Japan, 21-1, Toyama 1-chome, Shinjyuku-ku, Tokyo 162-8655, Japan*
[d] *Laboratory of Molecular and Cellular Biochemistry, Faculty of Dental Science, and Station for Collaborative Research, Kyushu University, Maidashi, Fukuoka 812-8582, Japan*
[e] *Biochemistry Division, National Cancer Center Research Institute, 1-1, Tsukiji 5-chome, Chuo-ku, Tokyo 104-0045, Japan*
[f] *Laboratory of Molecular Human Genetics, Faculty of Pharmaceutical Sciences, Kanazawa University, 13-1, Takara-machi, Kanazawa 920-0934, Japan*
[g] *Chemical Genetics Laboratory, RIKEN, Wako, Saitama 351-0198, Japan*
[h] *CREST Research Project, Japan Science and Technology Corporation, Saitama 332-0012, Japan*

Received 31 January 2004

Abstract

CDC25B is a dual-specificity phosphatase that activates CDK1/cyclin B. The nuclear exclusion of CDC25B is controlled by the binding of 14-3-3 to the nuclear export signal (NES) of CDC25B, which was reported to be amino acids H28 to L40 in the N-terminal region of CDC25B. In studying the subcellular localization of CDC25B, we found a functional NES at V52 to L65, the sequence of which is VTTLTQTMHDLAGL, where bold letters are leucine or hydrophobic amino acids frequently seen in an NES. The deletion of this NES sequence caused the mutant protein to locate exclusively in nuclei, while NES-fused GFP was detected in the cytoplasm. Moreover, the introduction of point mutations at some of the critical amino acids impaired cytoplasmic localization. Treatment with leptomycin B, a potent inhibitor of CRM1/exportin1, disrupted the cytoplasmic localization of both Flag-tagged CDC25B and NES-fused GFP. From these results, we concluded that the sequence we found is a bona fide NES of CDC25B.

Keywords: CDC25B; Nuclear export signal; Subcellular localization; GFP; 14-3-3; Leptomycin B

The activities of CDK (cyclin-dependent kinase) family proteins are regulated by associations with cyclin proteins and the phosphorylation–dephosphorylation cycle of CDK [1]. For instance, CDK1, which is necessary for the onset and maintenance of mitosis, is phosphorylated by Wee1/Myt1 kinases at threonine 14 and tyrosine 15 and is dephosphorylated by CDC25 family dual-specificity phosphatases. In higher eukaryotes, CDC25 phosphatases consist of three members, CDC25A, CDC25B, and CDC25C [2], and CDC25B is reported to have three isoforms, CDC25B1, -B2, and -B3, produced by alternative splicing [3]. Recent reports indicate that CDC25A plays a central role in cell cycle progression not only by regulating the G1 to S transition, but also by functioning in the G2 to M transition and M phase maintenance [4–7]. Furthermore, recent results of studies with CDC25B/CDC25C knock-out mice indicate that these proteins are not essential for development [8,9], supporting the idea that CDC25A is a prototype of the CDC25 family proteins. Unlike CDC25A, the functions of CDC25B and C are restricted to activating the CDK1/cyclin B1 complex, contributing to G2 to M traverse [2].

In spite of the non-essentiality of CDC25B in the mouse model, evidence has been accumulating that

* Corresponding author. Fax: +81-76-264-5989.
E-mail address: katsumi@kenroku.kanazawa-u.ac.jp (K. Yamashita).
[1] Present address: Research Institute for Radiation Biology and Medicine, Hiroshima University, 1-2-3 Kasumi, Minami-ku, Hiroshima 734-8553, Japan.

0006-291X/$ - see front matter © 2004 Elsevier Inc. All rights reserved.
doi:10.1016/j.bbrc.2004.02.039

CDC25B may have a positive function in tumorigenesis. First, CDC25B has an oncogenic role in cellular transformation [10]. Second, the over-expression of CDC25B has been reported in many primary human tumors and is correlated with a poor prognosis [11–15]. Third, transgenic mice over-expressing CDC25B in the mammary gland exhibited hyperplasia and susceptibility to carcinogen-induced mammary tumors [16,17]. Furthermore, the over-expression of CDC25B abrogated the G2/M checkpoint induced by DNA damage [6,18,19].

Recent reports indicate that the subcellular localization of CDC25B is controlled by the nuclear localization signal (NLS), the nuclear export signal (NES), and the association of 14-3-3 with Ser323, a specific site on CDC25B2 and B3 that corresponds to Ser309 of CDC25B1 [20,21]. The treatment of CDC25B-transfected cells with leptomycin B (LMB), a specific inhibitor of CRM1/exportin1 [22,23], abolishes its cytoplasmic localization, which indicates the presence of a functional NES in CDC25B [20].

During analyses of the control of cytoplasmic localization of CDC25B, we identified a functional NES on CDC25B at a site different from the published site [20]. In our study, deletion of the published NES region, from His28 to Leu40, did not influence the cytoplasmic localization of CDC25B; instead, a further deletion beyond Val52 impaired its cytoplasmic localization.

Materials and methods

Cell culture and transfection. HEK293 cells (ATCC No. CRL-1573) were cultured in Dulbecco's modified Eagle's medium (DMEM: Sigma, St. Louis, MO) supplemented with 10% fetal bovine serum (Invitrogen, USA), 100 U/ml penicillin, and 10 μg/ml streptomycin. Transient transfections were performed with FuGENE6 (Roche Diagnostics, Germany). For the indirect immunofluorescence experiments, cells were plated at the density of 2.0×10^5/well on a six-well plate 48 h before transfection, transfected with 3 μg FLAG-tagged CDC25B and then processed for immunostaining 24 h after transfection.

Plasmids. Human CDC25B (CDC25B1 subtype) cDNA was obtained from H. Okayama (Laboratory of Molecular Biology, Graduate School of Medicine, University of Tokyo, Japan). Venus/pCS2, which expresses a modified GFP, was provided by A. Miyawaki (Laboratory of Cell Function and Dynamics, Advanced Technology Development Center, Brain Science Institute, RIKEN, Japan). To express proteins as N-terminal FLAG-tagged forms, the pEF6/myc-HisB vector (Invitrogen, USA) was modified to contain two tandem arrays of the FLAG sequence between *Acc*65I and *Bam*HI sites. In this vector construct, the original *Acc*65I site was deleted and a new *Acc*65I site followed by an *Nde*I site was created in front of the *Bam*HI site. This modified vector was named pEF6/2× FLAG.

Constructing cDNA clones and site-directed mutagenesis. The coding sequence of CDC25B1 was amplified by PCR using primers B1-forward (5′- GGCCCCGGTACCATGGAGGTGCCCCAGCCG-3′, *Acc*65I site underlined) and B1-reverse (5′-GGCGCAGATATCTCACTGGT CCTGCAGCCG-3′, *Eco*RV site underlined).

After PCR amplification, DNA was digested with *Acc*65I and *Eco*RV and inserted into the pEF6/2× FLAG vector to be expressed in an N-terminal FLAG-tagged form. To introduce mutations into the human CDC25B cDNA (CDC25B1), the oligonucleotides listed below (and their complements) were used.

L32AAA: 5′-GGCCACCTCCCGGGCGCCGCAGCTGGATCT CATGGCCTC-3′
L74, 76A: 5′-AGCCGCCTGACGCAC GCATCCGCTTCTCG ACGGG CATCC-3′
L239AAA: 5′-AGCCCCCTGGCCGCAGGTCGCGCCTCTGCC ACCCCTGCAGAG-3′
V52A: 5′-GCTTCCTCGCCGGCCACCACCCTCACC-3′
V55A: 5′-CCGGTCACCACCGCC ACCCAGACCATG-3′
H60AAA: 5′-ACCCAGACCATGGCTGACGCAGCCGGGGCT GGCAGCCGCAGC-3′
L71A: 5′-AGCCGCAGCCGCGCAACGCACCTATCC-3′

N-terminal deletion mutants were produced by PCR using the following oligonucleotides as forward primers and the B1-reverse primer as the reverse primer (*Acc*65I site underlined):

Δ46: 5′-GGGTCCCCGGGTACCATGGCCGCTTCCTCGCCG GTCACC-3′
Δ51: 5′-GCCGCTGGTACCATGGTCACCACCCTCACCCAG ACC-3′
Δ54: 5′-ATAATAGGTACCATGCTCACCCAGACCATGCACG AC-3′
Δ56: 5′-ATAATAGGTACCATGCAGACCATGCACGACCTCG CCGGG-3′
Δ76: 5′-CTGACGCACGGTACCATGTCTCGACGGGCATCC GAATCC-3′

All the CDC25B mutant cDNAs were inserted between the *Acc*65I and *Eco*RV sites in the pEF6/2× FLAG vector for expression as N-terminal FLAG-tagged forms, as was done with the wild-type CDC25B1. The mutations were confirmed by sequencing.

The Venus-GFP coding sequence was excised from Venus/pCS2 with *Bam*HI and *Eco*RI and subcloned into the pEF6 vector to express the N-terminal 2× FLAG form of Venus-GFP. To make oligonucleotide-fused Venus-GFP cDNA, the oligonucleotides listed below (and their complements), each with an *Acc*65I sequence at the 5′-end and a *Bam*HI sequence at the 3′-end, were introduced between the FLAG sequence and Venus-GFP using *Acc*65I and *Bam*HI restriction sites. The sequences of these oligonucleotides were confirmed.

52–63: 5′-GTCACCACCCTCACCCAGACCATGCACGACCTC GCC-3′
52–66: 5′-GTCACCACCCTCACCCAGACCATGCACGACCTC GCCGGGCTCGGC-3′
52–73: 5′-GTCACCACCCTCACCCAGACCATGCACGACCTC GCCGGGCTCGGCAGCCGCAGCCGCCTGACGCAC-3′

Indirect immunofluorescence microscopy. Transfected HEK293 cells grown on glass coverslips were fixed in 3.7% formaldehyde in PBS and then permeabilized with 0.5% Triton X-100 in PBS. Venus-GFP and its fused proteins were detected following fixation. FLAG-tagged CDC25B and mutants were detected with rabbit polyclonal anti-FLAG antibody [24] and Alexa Fluor 594-conjugated goat anti-rabbit IgG (Molecular Probes, Eugene, OR). DNA was visualized using 0.1 μg/ml of 4′,6-diamidino-2-phenylindole (DAPI; Sigma, St. Louis, MO).

Results and discussion

Mutations in a possible NES of CDC25B1 did not induce nuclear localization

On the analysis of subcellular localization of CD C25B, we found CDC25B in nucleus or cytoplasm, which indicates that human CDC25B contains NES and NLS. Studies on the role of 14-3-3 subcellular localization of CDC25B have enabled us to conclude that

binding of 14-3-3 to CDC25B mobilizes CDC25B from nucleus to cytoplasm ([25] and our data will be published elsewhere). Experiments with *Xenopus* CDC25C, which has both NES and NLS, strongly suggest that the binding of 14-3-3 masks the NLS located downstream from the binding region, which would make nuclear export more active than import [26]. To assess 14-3-3 binding to CDC25B and its role in subcellular localization in detail, we examined spatial relationship between NES, NLS, and 14-3-3 binding site. CDC25B possesses typical bipartite NLS starting from Lys320. Contrary to NLS, it does not have typical NES such as $[Lx_{(1-3)}Lx_{(2-3)}LxL]$, where L stands for leucine or hydrophobic amino acids and x is any amino acids.

In order to identify NES in CDC25B, we first chose three leucine-rich, potential NES sequences: 28-*H*LPG*LLLGSHGLL*-40, 67-SRSR*LTHLSL*SRR-79, and 231-*V*EE*L*SP*LAL*GR*FSL*TP-246 (the bold italic letters are hydrophobic amino acids frequently observed in NES, Fig. 1A). One of the three sites, His28 to Leu40, was previously reported to be a functional NES [20]. Note that all three CDC25B sequences are conserved in the other two isotypes, CDC25B2 and -B3, although the numbering of the amino acids differs [3]. We introduced mutations at the critical leucine residues in these sequences. The mutation of Leu to Ala usually abolishes the function of a bona fide NES, and mutant proteins should be observed in nuclei. Contrary to this expectation, transiently expressed mutant clones, represented as L32AAA, L74/76A, and L239AAA (refer to Fig. 1A and its legend), did not exhibit specific nuclear localization (Figs. 1B and C). Moreover, these CDC25B1 mutant proteins localized in nuclei LMB-dependently. These results imply that CDC25B contains an NES in a region of other than those listed above, although His28 to Leu40 has been designated as the NES of CD C25B [20].

The functional NES of CDC25B1 starts at Val52

These results prompted us to find the functionally active NES in CDC25B. Therefore, we made a series of deletion mutants starting downstream from Leu40, since point mutations upstream from this had no effects on localization. First, we made a mutant with a deletion of the N-terminal 76 amino acids and expressed it as N-terminally FLAG-tagged CDC25B1. Surprisingly, the mutant localized exclusively in nuclei (Fig. 1D). The results strongly suggested that the functional NES of CDC25B1 occurs within the first 76 amino acids and that His28 to Leu40 is not relevant to the NES. Therefore, we created the following mutants with N-terminal deletions that started between Leu40 and Leu76: starting from Ala47 (Δ46 in Fig. 2), Val52 (Δ51), Leu55 (Δ54), and Gln57 (Δ56) (see Fig. 2A). These mutants were expressed as N-terminally FLAG-tagged forms to facilitate detection. On transfection with these mutants, the localization of proteins was observed, and their distribution was determined. As shown in Figs. 2B and C, the deletion of the first 51 amino acids did not affect cytoplasmic localization, but the deletion of the next three amino acids completely abolished the cytoplasmic localization of CDC25B1. These results imply that amino acid 52, 53, or 54 is crucial for cytoplasmic localization. Consulting the sequence, we tentatively concluded that Val52 was most likely the critical residue because the other two residues are threonine, which does not usually fulfill a function in an NES.

The NES of CDC25B1 localizes between Val52 and Leu66 and possesses LMB sensitivity

To determine the C-terminal end of the NES, several oligonucleotides encompassing Val52 to Leu71 were designed and attached to the 5′-end of Venus cDNA, a modified EGFP [27]. The N-terminal part of the construct was tagged with the 2× FLAG sequence for alternative detection of the protein. We made plasmids that contained Val52 to Ala63, Val52 to Gly66, and Val52 to His 73, designated 52–63, 52–66, and 52–73, respectively (Fig. 3A). The oligonucleotides contained Leu, which is usually critical to the function of an NES, although there is no typical NES sequence in this region at first glance.

These plasmids and FLAG-NES, which does not contain an insert and is referred to as Vector in Fig. 3, were transfected into HEK293 cells, and the localization of Venus-GFP protein was detected. As shown in Fig. 3B, GFP signals were detected uniformly in cells expressing FLAG-Venus and FLAG-Venus with amino acids Val52 to Ala63, called Vector and 52–63, respectively. Plasmid 52–66, in which the insert was extended by three C-terminal amino acids, gave rise to a GFP protein that localized in the cytoplasm. A further extended clone, 52–73, was also detected in the cytoplasm (Fig. 3B, 52–73). Therefore, we speculated that the functional NES of CDC25B1 is located between Val52 and Gly66 and that Leu65 is a critical C-terminal amino acid.

Next, we considered whether the NES we detected is LMB-sensitive. Transfectants of clone Venus (52–66) were treated with 20 ng/ml LMB for 3 h, and the localization of Venus-GFP was determined. As Fig. 3C shows, the cytoplasmic localization of Venus (52–66) is completely disturbed by LMB and it is evenly distributed throughout the cells. Therefore, we tentatively concluded that the amino acid sequence identified here is a new LMB-sensitive NES of CDC25B1.

Point mutations of hydrophobic amino acids in the NES abolish cytoplasmic localization

The LMB-sensitive NES contains functionally important hydrophobic amino acids, frequently Leu or